

Error Analysis of Bayesian Inverse Problems with Generative Priors

Bamdad Hosseini* and Ziqi Huang*

Abstract. Data-driven methods for the solution of inverse problems have become widely popular in recent years thanks to the rise of machine learning techniques. A popular approach concerns the training of a generative model on additional data to learn a bespoke prior for the problem at hand. In this article we present an analysis for such problems by presenting quantitative error bounds for minimum Wasserstein-2 generative models for the prior. We show that under some assumptions, the error in the posterior due to the generative prior will inherit the same rate as the prior with respect to the Wasserstein-1 distance. We further present numerical experiments that verify that aspects of our error analysis manifest in some benchmarks followed by an elliptic PDE inverse problem where a generative prior is used to model a non-stationary field.

Key words. Bayesian Inverse problems, Data-driven inference, Generative Models, Wasserstein Metric

AMS subject classifications. 62F15, 62G86, 49Q22.

1. Introduction. The Bayesian approach to inverse problems [57, 33] is now central to many computational frameworks in scientific computing and uncertainty quantification (UQ) [52, 70, 59]. In its most general form Bayes' rule is expressed in terms of the Radon-Nikodym derivative of the posterior measure with respect to the prior¹,

$$(1.1) \quad \frac{d\nu}{d\mu}(u) = \frac{1}{Z(y)} \exp(-\Phi(u; y)), \quad Z(y) = \mu(\exp(-\Phi(u; y))),$$

where u denotes the *unknown parameter* of interest that is assumed to be in a Banach space \mathcal{U} while y denotes the *observations or measurements* for the problem which may also belong to a Banach space \mathcal{Y} . The two are connected via the *likelihood potential* $\Phi : \mathcal{U} \times \mathcal{Y} \rightarrow \mathbb{R}$ (also known as the negative log-likelihood function) which encodes the likelihood of observing y given u . $\mu \in \mathbb{P}(\mathcal{U})$ is the *prior* probability measure, that encodes our prior knowledge about u while $\nu \in \mathbb{P}(\mathcal{U})$ is the *posterior* probability measure that represents an updated prior after observing y . Finally, $Z(y)$ is a normalizing constant referred to as the *evidence*, which ensures that ν is a well-defined probability measure.

Since the observations y are often limited and noisy, the exact recovery of u is impossible which motivates the use of Bayes' rule in the first place. Broadly speaking, if the observations y were not informative, then the likelihood potential Φ would be small, which means that many values of u can explain the observations. In this case we expect that the posterior ν would be close to the prior μ . Conversely, when the observations are very informative, we expect ν to concentrate around the true value of u . Many real-world applications of interest fall in the weakly or mildly informative observation regime, in which case, the prior has a

*University of Washington, Seattle, WA 98195, USA (bamdadh@uw.edu, ziqih2@uw.edu)

This work was supported by the National Science Foundation grants NSF-DMS-2208535 (Machine Learning for Bayesian Inverse Problems) and NSF-DMS-2337678 (CAREER: Gaussian Processes for Scientific Machine Learning: Theoretical Analysis and Computational Algorithms).)

¹We use the notation $\mu(f) = \int_{\mathcal{U}} f(u) \mu(du)$ for a probability measure μ and a measurable function f .

major influence on the shape and support of the posterior measure ν . It is precisely in these cases where the choice of the prior measure μ becomes extremely important as it directly influences the quality of the posterior as well as our UQ estimates in downstream tasks.

Hence, the design and choice of the prior μ is of great interest in the theory, application, and algorithmic development of Bayesian inverse problems (BIPs). Traditionally, the priors are designed by experts by balancing theoretical and algorithmic convenience with the specific needs of the problem at hand; see for example [21] or [33, Sec. 3.3] as well as Subsection 1.2. However, in the past decade, thanks to the rise of machine learning (ML) and generative modeling, a new class of methodologies have been proposed where the prior μ is learned or designed in an adaptive manner. This class largely falls under the category of data-driven methods for solving inverse problems in the parlance of [5, 47, 45].

We can categorize data-driven inversion methods under three broad families: (1) learned prior models, where an ML model is trained on an additional empirical data set to learn an empirical prior $\hat{\mu}$ in the Bayesian context or equivalently a regularizer in the deterministic context [10, 42, 44, 9, 51, 47]; (2) plug-and-play priors that utilize denoising operators to learn algorithmic priors and regularizers [62, 72, 71, 38]; and (3) the more recent class of simulation-based inference methods that circumvent the need for explicit knowledge of the likelihood potential or the prior measure and only require black-box methods that can sample the prior and simulate the observations [41, 55, 7, 67]. Our goal in this article is to develop an error analysis for the first class of BIP methods that utilize a learned prior, perhaps using a generative model.

1.1. Problem statement and summary of contributions. We consider an approximation to (1.1) of the form

$$(1.2) \quad \frac{d\hat{\nu}}{d\hat{\mu}}(u) = \frac{1}{\hat{Z}(y)} \exp(-\Phi(u; y)), \quad \hat{Z}(y) = \hat{\mu}(\exp(-\Phi(u; y))),$$

where $\hat{\nu}$ is an approximate posterior measure that arises due to an approximate prior $\hat{\mu}$ —note that we have assumed that the likelihood potential Φ is fixed as we are primarily interested in prior approximations, although we will discuss likelihood perturbations later. We further assume that $\hat{\mu}$ is defined as the pushforward of a reference measure $\eta \in \mathbb{P}(\mathcal{U})$, that is, $\hat{\mu} = \hat{T}\#\eta$, where $\#$ denotes the pushforward operator² and $\hat{T} : \mathcal{U} \rightarrow \mathcal{U}$ is a transport map which represents a generative model. The transport model encompasses many popular generative models including Generative Adversarial Nets (GANs) [22], Normalizing flows (NFs) [36], and Flow Matching [40].

Our primary goal is to quantify the error between the approximate posterior $\hat{\nu}$ and the true posterior ν , due to the limitations in computing \hat{T} arising from finite training data and limited parameterizations.

We emphasize that we are mainly concerned here with the approximation of the posterior ν due to the approximation of the prior μ with the generative model $\hat{\mu}$, that is, we view μ as a ground truth prior that the generative model targets and so we are not concerned with the

²Given a measure $\eta \in \mathbb{P}(\mathcal{U})$ and a measurable map $T : \mathcal{U} \rightarrow \mathcal{V}$, we define $T\#\eta \in \mathbb{P}(\mathcal{V})$ via the identity $T\#\eta(A) = \eta(T^{-1}(A))$ for any measurable set A with $T^{-1}(A)$ denoting the pre-image of A under T .

performance of the true posterior ν in terms of its concentration around the true value of the unknown parameter u .

We make the following four contributions towards the above goal in the setting where $\mathcal{U} \subseteq \mathbb{R}^d$ for $d \geq 1$:

- (i) Writing \mathcal{W}_p for $p = 1, 2$ to denote the Wasserstein- p distance (see [Subsection 2.2](#) for definition) we prove a generic bound of the form

$$\mathcal{W}_1(\nu, \hat{\nu}) \leq C_{\text{stab}} \mathcal{W}_2(\mu, \hat{\mu}),$$

where $C_{\text{stab}} > 0$ is a constant that depends on regularity of the likelihood Φ and some moments of μ and $\hat{\mu}$. The precise result is given in [Theorem 2.2](#) building on [\[56, 20\]](#).

- (ii) Consider any map $\hat{T} \in \arg \min_{T \in \hat{\mathcal{T}}} \mathcal{W}_2(T \# \eta, \mu^N)$, where $\hat{\mathcal{T}}$ denotes an approximation class such as neural nets or polynomials, and μ^N denotes the empirical measure associated with N i.i.d. samples from μ . We then prove, under appropriate assumptions, that for any $\varepsilon > 0$ and with probability $1 - CN^{-1/d}/\varepsilon$ (with some constant $C > 0$) it holds that

$$\mathcal{W}_2(\hat{\mu}, \mu) \lesssim \inf_{T \in \hat{\mathcal{T}}} \|T - T^\dagger\|_{L_\eta^2} + \varepsilon,$$

where \lesssim contains independent constants and T^\dagger is any map that satisfies $T^\dagger \# \eta = \mu$. The precise statement is given in [Subsection 3.1](#).

- (iii) Under further assumptions we extend the above bound to the posteriors, showing that in the same high-probability event, we have

$$\mathcal{W}_1(\hat{\nu}, \nu) \lesssim \inf_{T \in \hat{\mathcal{T}}} \|T - T^\dagger\|_{L_\eta^2} + \varepsilon + \delta$$

where $\delta > 0$ is an additional bias term that encodes the tail properties of the prior μ . The precise statement can be found in [Subsection 3.2](#).

- (iv) Finally, we present a number of numerical experiments aimed at verifying our theoretical bounds, in particular the result of item (i). We also present a nonlinear PDE inverse problem with a generative prior that elucidates the benefits of using generative priors to enhance the performance of simple Markov chain Monte Carlo (MCMC) methods for solving high-dimensional BIPs with highly non-Gaussian priors.

1.2. Literature Review. We focus our review of the relevant literature to recent works on data-driven techniques for inverse problems. For a general overview of the Bayesian approach to inverse problems we refer the reader to [\[57, 33\]](#).

Data-driven approaches to inverse problems. Data-driven approaches to inverse problems became popular in the last decade alongside the wide adoption of ML techniques for imaging [\[5\]](#). Many data-driven approaches were widely used in inverse problems in the past, most notably, reduced order models [\[14\]](#) and emulators [\[34\]](#) for likelihoods and forward maps. However, the more modern data-driven techniques are focused on the automated modeling of prior information. As opposed to classic inverse problems, where one often employs a smoothness prior, e.g. Tikhonov regularization [\[65\]](#), here side information or data is assumed to be

available that can be used to enhance the prior. We already mentioned the three classes of data-driven priors: (1) learned priors [10, 42, 44, 9, 51, 47, 16, 18, 24]; plug-and-play priors [62, 72, 71, 38]; and simulation-based inference methods [41, 55, 7, 67].

Our work is focused on the analysis of algorithms for class (1) where we assume there exists, a priori, a data set of "typical" possible choices of the unknown parameter, e.g., a collection of MRI or CT images. Then the goal of data-driven inference is to build a bespoke prior for this data set, often using a generative model. While algorithmic and methodological developments in this space have attracted a lot of attention, to our knowledge the theoretical analysis of inverse problems with generative or adaptive priors remains limited. Previous works [10, 53, 32, 1] considered the "compressed sensing" setting where the forward map is linear (typically a random matrix) and the prior is generative, and give theoretical results and guarantees on the recovery of the latent representation of the parameters in the domain of the generative prior. While [32, 1] have the closest analysis to our work, namely considering Wasserstein perturbations of the prior, their theory remains limited to linear forward maps and gives recovery guarantees for the parameter provided that the prior is "good enough" in a Wasserstein sense. In comparison, our theory is simple and covers both linear and nonlinear problems as it directly quantifies the error in approximating the posterior measure due to learning the prior. We do not give recovery guarantees, however, our convergence results for the priors can be combined with the results in [32, 1] to further understand when their recovery guarantees hold.

Our analysis also has some bearing on class (3) methodologies, that is, amortized or simulation-based inference [7, 26, 2, 4, 48]. Broadly speaking, these models utilize existing or simulated data sets of pairs of parameters u and data y to directly learn a conditional generative model for the posterior ν . While the prior μ is never explicitly identified or learned from data, it is implicitly learned through the data set often using similar generative models that are used to learn the priors in other types of data-driven inverse problems. Hence, we conjecture that our type of analysis can be extended to such conditional generative models, as is done in [2] for the case of triangular OT maps.

Error analysis of generative models. The error analysis of generative models has attracted a lot of attention in recent years, most notably the works [39, 61, 60, 29, 54], where the estimation error of GANs were studied, as well as the more recent body of work on the error analysis of flow and diffusion models [3, 8, 28, 43, 50]. The error analysis of transport models, such as those used in our work, has been done in various contexts: an abstract framework for the error analysis of generic transport models was developed in [6] while [31, 66, 68, 69] studied triangular maps, also known as Knothe-Rosenblatt maps, and the works [30, 17, 12, 2] developed the statistical analysis of optimal transport maps with quadratic costs. Despite these works the broader approximation theory of transport-based generative modeling is far from complete and the combination of these results with data-driven inverse problems, such as our work in this paper, remains largely open.

Perturbation theory of BIPs. The perturbation theory of BIPs is a cornerstone of our theoretical analysis of data-driven BIPs since such an analysis is inevitable when learned priors or likelihoods are involved. Historically, this perturbation analysis appeared in the context of the well-posedness of BIPs with early works focusing on Gaussian priors, see [57, 15] and references within, followed by extensions to non-Gaussian priors [27, 25, 58, 37]. While these

works primarily considered the perturbation of BIPs with respect to likelihood functions the paper [56] extended that analysis to prior perturbations with respect to various metrics including the Wasserstein distances which are crucial to our analysis here. However, that analysis required a global Lipschitz assumption on the likelihood which does not hold for many practical problems including least squares problems. The manuscript [20] extended that analysis to bespoke optimal transport metrics that could handle only locally Lipschitz likelihoods and included a quantitative analysis of BIPs with generative priors that forms the foundation of our analysis in this paper.

1.3. Outline. The rest of the article is organized as follows: [Section 2](#) outlines a perturbation analysis for Bayesian posterior measures with respect to the Wasserstein-1 distance, giving technical results that we use later in the paper; [Section 3](#) presents our main theoretical results and in particular the quantitative error bounds for learned priors and subsequent posteriors; [Section 4](#) presents our numerical experiments that investigate and extend our theory; and [Section 5](#) outlines our concluding remarks and discussions.

2. Posterior perturbations with respect to the Wasserstein-1 distance. Below we outline general perturbations results for BIPs that serve as the foundation for our error analysis later on. We begin with preliminary results from [20, 56] in [Subsection 2.1](#) which we then tailor to the case of the Wasserstein-1 distance in [Subsection 2.2](#). Throughout this section we mostly consider the data y to be fixed, but we comment on the dependence of our bounds on the data and how it can be controlled for additive noise models in [Theorem 2.4](#)

2.1. Perturbation bounds with respect to integral probability metrics. Consider separable Banach spaces \mathcal{U}, \mathcal{Y} along with the spaces of Borel probability measures on them, denoted by $\mathbb{P}(\mathcal{U})$ and respectively $\mathbb{P}(\mathcal{Y})$. For a continuous and positive cost $c : \mathcal{U} \times \mathcal{U} \rightarrow \mathbb{R}_{\geq 0}$ define the space

$$\text{Lip}_c(\mathcal{U}) := \{ \psi : \mathcal{U} \rightarrow \mathbb{R} \mid |\psi(u) - \psi(u')| \leq c(u, u'), \quad \forall u, u' \in \mathcal{U} \},$$

and further define the statistical divergence (also called an integral probability metric [46])

$$\mathcal{D}_c : \mathbb{P}(\mathcal{U}) \times \mathbb{P}(\mathcal{U}) \rightarrow \mathbb{R}_{\geq 0} \cup \{+\infty\}, \quad \mathcal{D}_c(\gamma, \gamma') := \sup_{\psi \in \text{Lip}_c(\mathcal{U})} \gamma(\psi) - \gamma'(\psi).$$

Note that \mathcal{D}_c is not a true metric since it may not be definite, i.e., $\mathcal{D}_c(\gamma, \gamma') = 0$ does not imply that $\gamma = \gamma'$, though it always satisfies the triangle inequality.

For a measure $\mu \in \mathbb{P}(\mathcal{U})$, continuous functions $f : \mathcal{U} \rightarrow \mathbb{R}_{\geq 0}$, $h : \mathcal{U} \times \mathcal{Y} \rightarrow \mathbb{R}_{> 0}$, and $\ell : \mathcal{U} \times \mathcal{U} \times \mathcal{Y} \rightarrow \mathbb{R}_{\geq 0}$, and a locally bounded function $g : \mathcal{Y} \rightarrow \mathbb{R}_{> 0}$, we define the class

$$\begin{aligned} \mathcal{F}(f, g, h, \ell, \mu) := & \left\{ \Phi : \mathcal{U} \times \mathcal{Y} \rightarrow \mathbb{R} \mid \Phi(\cdot; y) \in L^1(\mu), \text{ for all } y \in \mathcal{Y}, \right. \\ & \text{and } -\log f(u) - \log g(y) \leq \Phi(u; y) \leq -\log h(u, y), \\ & \left. \text{and } |\Phi(u; y) - \Phi(u'; y)| \leq \ell(u, u', y) \|u - u'\|_{\mathcal{U}} \right\}. \end{aligned}$$

With this setup we now recall the following result from [20] concerning the perturbation of posterior measures with respect to the priors:

Proposition 2.1. *Consider priors $\mu, \hat{\mu} \in \mathbb{P}(\mathcal{U})$, a likelihood $\Phi \in \mathcal{F}(f, g, h, \ell, \mu)$, and a continuous and positive cost $c : \mathcal{U} \times \mathcal{U} \rightarrow \mathbb{R}_{\geq 0}$. Further suppose that $f, fc(\cdot, 0) \in L^1(\mu)$ and $h(\cdot, y) \in L^1(\mu) \cap L^1(\hat{\mu})$ for all $y \in \mathcal{Y}$. Then it holds that*

$$\mathcal{D}_c(\nu, \hat{\nu}) \leq g^2(y) \left[\frac{\|f\|_{L^1(\mu)} + \|fc(\cdot, y)\|_{L^1(\mu)}}{\|h(\cdot, y)\|_{L^1(\mu)} \|h(\cdot, y)\|_{L^1(\hat{\mu})}} \right] \mathcal{D}_{c_y}(\mu, \hat{\mu}),$$

where $\nu, \hat{\nu}$ are given by (1.1) and (1.2) respectively and $c_y : \mathcal{U} \times \mathcal{U} \rightarrow \mathbb{R}_{\geq 0}$ is a new cost given by the expression

$$c_y(u, u') := [1 \vee c(u, 0) \vee c(u', 0)] \cdot [f(u) \vee f(u')] \cdot [1 \vee \ell(u, u', y)] \cdot c(u, u'), \quad \forall u, u' \in \mathcal{U}.$$

The above proposition is central to our exposition in the rest of the paper as it allows us to control the error between two posterior measures in terms of the underlying priors although we note that the divergences on both sides of the inequality are different and the cost c_y often leads to a stronger metric than the original one chosen to measure the posterior perturbations. We also emphasize that the cost c_y depends on the observed data y through the function ℓ which encodes the local Lipschitz constant of the likelihood Φ .

2.2. Perturbation bounds with respect to Wasserstein distances. We now tailor the result of (2.1) to the setting of Wasserstein distances. For $p \in [1, +\infty)$ let us write $\mathbb{P}^p(\mathcal{U}) := \{\gamma \in \mathbb{P}(\mathcal{U}) \mid \gamma(\|\cdot\|^p) < +\infty\}$, i.e., probability measures with bounded p moments. Then we recall the definition of the Wasserstein- p distances from [63]:

$$(2.1) \quad \mathcal{W}_p(\gamma, \gamma') := \left(\inf_{\pi \in \Pi(\gamma, \gamma')} \int_{\mathcal{U} \times \mathcal{U}} \|u - u'\|_{\mathcal{U}}^p \pi(du, du') \right)^{1/p}, \quad \forall \gamma, \gamma' \in \mathbb{P}^p(\mathcal{U}),$$

where $\Pi(\gamma, \gamma') \subset \mathbb{P}(\mathcal{U} \times \mathcal{U})$ denotes the space of couplings of γ and γ' , i.e., measures defined on the product space $\mathcal{U} \times \mathcal{U}$ whose first marginal coincides with γ and their second marginals coincide with γ' :

$$\Pi(\gamma, \gamma') := \left\{ \pi \in \mathbb{P}(\mathcal{U} \times \mathcal{U}) \mid \int_{\mathcal{U}} \pi(\cdot, du) = \gamma, \quad \int_{\mathcal{U}} \pi(du, \cdot) = \gamma' \right\}.$$

By convention we set $\mathcal{W}_p(\gamma, \gamma') = +\infty$ if either measure does not belong to $\mathbb{P}^p(\mathcal{U})$. By the celebrated Kantorovich duality [63, Thm. 5.10 and Case. 5.16] for the particular case $p = 1$ we have the equivalent expression

$$(2.2) \quad \mathcal{W}_1(\gamma, \gamma') = \sup_{\psi \in \text{Lip}(\mathcal{U})} \gamma(\psi) - \gamma'(\psi),$$

where we wrote $\text{Lip}(\mathcal{U}) := \{\psi : \mathcal{U} \rightarrow \mathbb{R} \mid |\psi(u) - \psi(u')| \leq \|u - u'\|_{\mathcal{U}}\}$. In other words, $\mathcal{W}_1 = \mathcal{D}_c$ for the cost $c(u, u') = \|u - u'\|_{\mathcal{U}}$. Indeed, a straightforward calculation shows that for the cost functions $c(u, u') = \|u - u'\|_{\mathcal{U}}^p$ we have the inequality

$$(2.3) \quad \mathcal{D}_c(\gamma, \gamma') \leq \mathcal{W}_p^p(\gamma, \gamma'),$$

showing that the \mathcal{D}_c divergences are weaker than the Wasserstein distances. More broadly, for any cost c we also have the inequality

$$(2.4) \quad \mathcal{D}_c(\gamma, \gamma') \leq \inf_{\pi \in \Pi(\gamma, \gamma')} \int_{\mathcal{U} \times \mathcal{U}} c(u, u') \pi(du, du') =: \mathcal{W}_c(\gamma, \gamma').$$

We are now ready to present our first main theoretical results which allows us to control the \mathcal{W}_1 distance between posteriors in terms of the \mathcal{W}_2 distance between the priors. Our result extends those given in [56, Sec. 5] and [20, Sec. 4.3] to the case of likelihoods that are not globally Lipschitz.

Theorem 2.2. *Consider priors $\mu, \hat{\mu} \in \mathbb{P}^2(\mathcal{U})$ and a likelihood $\Phi \in \mathcal{F}(f, g, h, \ell, \mu)$. Further suppose $(1 + \|\cdot\|_{\mathcal{U}})f \in L^1(\mu)$ and $h(\cdot, y) \in L^1(\mu) \cap L^1(\hat{\mu})$ for all $y \in \mathcal{Y}$. Then it holds that*

$$(2.5) \quad \mathcal{W}_1(\nu, \hat{\nu}) \leq C_{\text{stab}}(y) \mathcal{W}_2(\mu, \hat{\mu}),$$

where the constant $C_{\text{stab}}(y)$ has the explicit form

$$(2.6) \quad C_{\text{stab}}(y) = g^2(y) \left[\frac{\|(1 + \|\cdot\|_{\mathcal{U}})f\|_{L^1(\mu)}}{\|h(\cdot, y)\|_{L^1(\mu)} \|h(\cdot, y)\|_{L^1(\hat{\mu})}} \right] \times \left(\int_{\mathcal{U} \times \mathcal{U}} [1 \vee \ell(u, v, y)]^2 \cdot [f(u) \vee f(v)]^2 \cdot [1 \vee \|u\|_{\mathcal{U}} \vee \|v\|_{\mathcal{U}}]^2 \pi^*(du, dv) \right)^{\frac{1}{2}}.$$

Here π^* denotes the Wasserstein-2 optimal coupling between μ and $\hat{\mu}$.

Proof. Since $\Phi \in \mathcal{F}(f, g, h, \ell, \mu)$, and $f, f \cdot \|\cdot\|_{\mathcal{U}} \in L^1(\mu)$, by Theorem 2.1 along with (2.2), we obtain the bound

$$(2.7) \quad \mathcal{W}_1(\nu, \hat{\nu}) \leq \frac{g^2(y) [\|f\|_{L^1(\mu)} + \|f \cdot \|\cdot\|_{\mathcal{U}}\|_{L^1(\mu)}]}{\|h(\cdot, y)\|_{L^1(\mu)} \|h(\cdot, y)\|_{L^1(\hat{\mu})}} \mathcal{D}_{c_y}(\mu, \hat{\mu}),$$

where c_y is defined as:

$$c_y(u, v) = [1 \vee \|u\|_{\mathcal{U}} \vee \|v\|_{\mathcal{U}}] \cdot [f(u) \vee f(v)] \cdot [1 \vee \ell(u, v, y)] \cdot \|u - v\|_{\mathcal{U}}.$$

We can simplify (2.7) by observing $\|f\|_{L^1(\mu)} + \|f \cdot \|\cdot\|_{\mathcal{U}}\|_{L^1(\mu)} = \|(1 + \|\cdot\|_{\mathcal{U}})f\|_{L^1(\mu)}$ since f is positive. Moreover, an application of (2.4) yields $\mathcal{D}_{c_y}(\mu, \hat{\mu}) \leq \mathcal{W}_{c_y}(\mu, \hat{\mu})$. We now bound the right hand side of this expression by the Wasserstein-2 distance between μ and $\hat{\mu}$. By the Cauchy-Schwarz inequality, for any $\pi \in \Pi(\mu, \hat{\mu})$ we have the bound

$$\begin{aligned} & \int_{\mathcal{U} \times \mathcal{U}} c_y(u, v) \pi(du, dv) \\ & \leq \left(\int_{\mathcal{U} \times \mathcal{U}} [1 \vee \ell(u, v, y)]^2 \cdot [f(u) \vee f(v)]^2 \cdot [1 \vee \|u\|_{\mathcal{U}} \vee \|v\|_{\mathcal{U}}]^2 \pi(du, dv) \right)^{\frac{1}{2}} \\ & \quad \times \left(\int_{\mathcal{U} \times \mathcal{U}} |u - v|^2 \pi(du, dv) \right)^{\frac{1}{2}}. \end{aligned}$$

Let $\pi^*(u, v) = \arg \min_{\pi \in \Pi(\mu, \hat{\mu})} \int_{\mathcal{U} \times \mathcal{U}} |u - v|^2 \pi(du, dv)$ be the optimal Wasserstein-2 coupling and apply the above bound to get

$$\begin{aligned} \mathcal{W}_{c_y}(\mu, \hat{\mu}) &\leq \int_{\mathcal{U} \times \mathcal{U}} c_y(u, v) \pi^*(du, dv) \\ &\leq \left(\int_{\mathcal{U} \times \mathcal{U}} [1 \vee \ell(u, v, y)]^2 \cdot [f(u) \vee f(v)]^2 \cdot [1 \vee \|u\|_{\mathcal{U}} \vee \|v\|_{\mathcal{U}}]^2 \pi^*(du, dv) \right)^{\frac{1}{2}} \mathcal{W}_2(\mu, \hat{\mu}). \end{aligned}$$

Combining this bound with (2.7) completes the proof. \blacksquare

Let us now outline a corollary to the above result for the case of additive Gaussian noise models that are commonly used in practice.

Corollary 2.3. *Consider priors $\mu, \hat{\mu}$ and the quadratic likelihood potential*

$$(2.8) \quad \Phi(u; y) = \frac{1}{2\sigma^2} \|F(u) - y\|_{\mathcal{Y}}^2,$$

arising from the model $y = F(u) + \xi$, $\xi \sim N(0, \sigma^2 I)$, where $F : \mathcal{U} \rightarrow \mathcal{Y}$ is locally Lipschitz such that

$$\|F(u) - F(u')\|_{\mathcal{Y}} \leq \ell_F(u, u') \|u - u'\|_{\mathcal{U}}, \quad \forall u, u' \in \mathcal{U},$$

for some function $\ell_F : \mathcal{U} \times \mathcal{U} \rightarrow \mathbb{R}_{\geq 0}$. Further suppose $\exp(-\frac{1}{\sigma^2} \|F(\cdot)\|_{\mathcal{Y}}^2) \in L^1(\mu) \cap L^1(\hat{\mu})$. Then (2.5) holds with

$$(2.9) \quad \begin{aligned} C_{\text{stab}}(y) &= \left[\frac{\exp\left(\frac{2}{\sigma^2} \|y\|_{\mathcal{Y}}^2\right) (1 + \mu(\|\cdot\|_{\mathcal{U}}))}{\mu \left(\exp\left(-\frac{1}{\sigma^2} \|F(\cdot)\|_{\mathcal{Y}}^2\right)\right) \hat{\mu} \left(\exp\left(-\frac{1}{\sigma^2} \|F(\cdot)\|_{\mathcal{Y}}^2\right)\right)} \right] \\ &\quad \times \left(\int_{\mathcal{U} \times \mathcal{U}} \left[1 \vee \left(\frac{1}{2\sigma^2} \ell_F(u, v) (\|F(u)\|_{\mathcal{Y}} + \|F(v)\|_{\mathcal{Y}} + 2\|y\|_{\mathcal{Y}}) \right)^2 \right] \right. \\ &\quad \left. \cdot \left[1 \vee \|u\|_{\mathcal{U}} \vee \|v\|_{\mathcal{U}} \right]^2 \pi^*(du, dv) \right)^{\frac{1}{2}}. \end{aligned}$$

Proof. Since Φ is positive we can take $f = g = 1$. Moreover, by the triangle inequality

$$\frac{1}{2\sigma^2} \|F(u) - y\|_{\mathcal{Y}}^2 \leq \frac{1}{\sigma^2} (\|F(u)\|_{\mathcal{Y}}^2 + \|y\|_{\mathcal{Y}}^2) = -\log h(u, y).$$

To show Φ is locally Lipschitz, consider

$$\begin{aligned} 2\sigma^2 \|\Phi(u; y) - \Phi(u'; y)\| &= \|\|F(u) - y\|_{\mathcal{Y}}^2 - \|F(u') - y\|_{\mathcal{Y}}^2\| \\ &= (\|F(u) - y\|_{\mathcal{Y}} - \|F(u') - y\|_{\mathcal{Y}})(\|F(u) - y\|_{\mathcal{Y}} + \|F(u') - y\|_{\mathcal{Y}}) \\ &\leq \|F(u) - F(u')\|_{\mathcal{Y}} (\|F(u) - y\|_{\mathcal{Y}} + \|F(u') - y\|_{\mathcal{Y}}) \\ &\quad \text{(By reverse triangle inequality)} \\ &\leq \ell_F(u, u') \|u - u'\|_{\mathcal{U}} (\|F(u)\|_{\mathcal{Y}} + \|F(u')\|_{\mathcal{Y}} + 2\|y\|_{\mathcal{Y}}) \\ &\quad \text{(By triangle inequality)} \end{aligned}$$

Since F is locally Lipschitz then F is also locally bounded which implies that Φ is locally Lipschitz with $\ell(u, u', y) = \frac{1}{2\sigma^2} \ell_F(u, u')(\|F(u)\|_{\mathcal{Y}} + \|F(u')\|_{\mathcal{Y}} + 2\|y\|_{\mathcal{Y}})$. An application of [Theorem 2.2](#) and simplifying the expression for the constants yields the desired result. \blacksquare

Remark 2.4. We note that the constant C_{stab} in [\(2.9\)](#) is dependent on the data y . It is helpful to try to simplify this expression to further highlight the dependence of the stability constant of the data as this is often crucial in the study of the consistency and sensitivity of BIPs to noise in the data [\[49\]](#). To this end, assuming suitable integrability conditions we can write

$$\begin{aligned}
& \int_{\mathcal{U} \times \mathcal{U}} \left[1 \vee \left(\frac{1}{2\sigma^2} \ell_F(u, v)(\|F(u)\|_{\mathcal{Y}} + \|F(v)\|_{\mathcal{Y}} + 2\|y\|_{\mathcal{Y}}) \right)^2 \right] \cdot [1 \vee \|u\|_{\mathcal{U}} \vee \|v\|_{\mathcal{U}}]^2 \pi^*(du, dv) \\
& \lesssim \int_{\mathcal{U} \times \mathcal{U}} \left[1 + \frac{1}{\sigma^4} \ell_F^2(u, v)(\|F(u)\|_{\mathcal{Y}} + \|F(v)\|_{\mathcal{Y}} + 2\|y\|_{\mathcal{Y}})^2 \right] \cdot [1 \vee \|u\|_{\mathcal{U}}^2 \vee \|v\|_{\mathcal{U}}^2] \pi^*(du, dv) \\
& \lesssim \int_{\mathcal{U} \times \mathcal{U}} \left[1 + \frac{1}{\sigma^4} \ell_F^2(u, v)(\|F(u)\|_{\mathcal{Y}} + \|F(v)\|_{\mathcal{Y}})^2 + \frac{1}{\sigma^4} \ell_F^2(u, v)^2 \|y\|_{\mathcal{Y}}^2 \right] \\
& \quad \cdot [1 + \|u\|_{\mathcal{U}}^2 + \|v\|_{\mathcal{U}}^2] \pi^*(du, dv) \\
& \lesssim \int_{\mathcal{U} \times \mathcal{U}} \left[1 + \frac{1}{\sigma^4} \ell_F^2(u, v)(\|F(u)\|_{\mathcal{Y}}^2 + \|F(v)\|_{\mathcal{Y}}^2) \right] \cdot [1 + \|u\|_{\mathcal{U}}^2 + \|v\|_{\mathcal{U}}^2] \pi^*(du, dv) \\
& \quad + \left[\frac{1}{\sigma^4} \|y\|_{\mathcal{Y}}^2 \right] \int_{\mathcal{U} \times \mathcal{U}} \ell_F(u, v)^2 \cdot [1 + \|u\|_{\mathcal{U}}^2 + \|v\|_{\mathcal{U}}^2] \pi^*(du, dv) \\
& =: \left(1 + \frac{1}{\sigma^4} \right) (\alpha + \alpha' \|y\|_{\mathcal{Y}}^2),
\end{aligned}$$

where we repeatedly used the identity $(a+b)^2 \leq 2(a^2+b^2)$ and \lesssim contains a universal constant that is independent of σ . We note that $\alpha, \beta > 0$ are constants that depend only on the growth rate of F and ℓ_F and effectively translate to moment conditions on π^* . To this end, we can explicitly characterize the dependence of C_{stab} in terms of y as

$$C_{\text{stab}}(y) \lesssim \alpha'' \left(1 + \frac{1}{\sigma^2} \right) \exp \left(\frac{2}{\sigma^2} \|y\|_{\mathcal{Y}}^2 \right) (1 + \|y\|_{\mathcal{Y}}),$$

where once again $\alpha'' > 0$ depends only on the moments of π^* . Let us now write $v \in \mathbb{P}(\mathcal{Y})$ for the marginal distribution of y under the prior, i.e., $v = F\#\mu * N(0, \sigma^2 I)$. Then we have the bound

$$\mathbb{E}_{y \sim v} \mathcal{W}_1(\nu, \hat{\nu}) \lesssim \alpha'' \left(1 + \frac{1}{\sigma^2} \right) v \left((1 + \|y\|_{\mathcal{Y}}) \exp \left(\frac{2}{\sigma^2} \|y\|_{\mathcal{Y}}^2 \right) \right) \mathcal{W}_2(\mu, \hat{\mu}).$$

Thus the average \mathcal{W}_1 distance between the posteriors is controlled by the prior \mathcal{W}_2 distance provided that the marginal v has sufficiently light tails and the prior has sufficient bounded moments so that $\alpha'' < +\infty$. \diamond

3. Error analysis of BIPs with generative priors. In this section we build on the perturbation bounds in [Section 2](#) to give quantitative bounds for posteriors that arise from generative

priors that can be modeled as transport maps. We begin by controlling the errors of the generative priors in [Subsection 3.1](#) followed by the extension to error bounds for the posteriors in [Subsection 3.2](#) that constitute our main results. We note that throughout this section we assume that the data y is fixed and only consider the errors due to the prior generative models. At various points we provide further remarks on how one could extend our results to contain perturbations of the data y .

3.1. Prior bounds. We begin by deriving error bounds for the prior measures, i.e., a bound on $\mathcal{W}_2(\mu, \hat{\mu})$ where take $\hat{\mu}$ to be a generative prior and μ to be the ground truth prior. To this end, we consider the model

$$(3.1) \quad \hat{\mu}^{N,M} := \hat{T}^{N,M} \# \eta, \quad \hat{T}^{N,M} := \arg \min_{T \in \hat{\mathcal{T}}} \mathcal{W}_2(T \# \eta^M, \mu^N),$$

where η^M, μ^N are empirical approximations to η and μ with M and N samples respectively and $\hat{\mathcal{T}}$ is an approximation class of maps $T : \mathcal{U} \rightarrow \mathcal{U}$ that models our generative model class, such as neural nets of a certain size, polynomials, or reproducing kernel Hilbert spaces (RKHSs). Our goal in this subsection is to bound $\mathcal{W}_2(\mu, \hat{\mu}^{M,N})$.

To simplify our analysis, we first consider the slightly simpler problem

$$(3.2) \quad \hat{\mu}^N := \hat{T}^N \# \eta, \quad \hat{T}^N := \arg \min_{T \in \hat{\mathcal{T}}} D(T \# \eta, \mu^N),$$

where we only use the empirical prior μ^N to train the generative model and use the exact reference η ³. Throughout this section we assume $\hat{\mathcal{T}} \subset L^2(\eta)$ and further assume there exists a ground truth map $T^\dagger \in L^2(\eta)$ such that $\mu = T^\dagger \# \eta$. Finally, we take $d \geq 4$ to simplify our statements later on.

Our first result is a technical lemma that allows us to decompose the error of $\hat{\mu}^N$ into an approximation bias, due to the choice of $\hat{\mathcal{T}}$ and a stochastic error due to finite samples.

Lemma 3.1. *Consider (3.2) and define*

$$(3.3) \quad \hat{T}^\dagger := \arg \min_{T \in \hat{\mathcal{T}}} \|T - T^\dagger\|_{L^2(\eta)}.$$

Then it holds that $\mathcal{W}_2(\hat{\mu}^N, \mu) \leq \|\hat{T}^\dagger - T^\dagger\|_{L^2(\eta)} + 2\mathcal{W}_2(\mu, \mu^N)$.

Proof. We can then write the sequence of inequalities

$$(3.4) \quad \begin{aligned} \mathcal{W}_2(\hat{T}^N \# \eta, \mu) &\leq \mathcal{W}_2(\hat{T}^N \# \eta, \mu^N) + \mathcal{W}_2(\mu, \mu^N) \quad (\text{By the Triangle Inequality}) \\ &\leq \mathcal{W}_2(\hat{T}^\dagger \# \eta, \mu^N) + \mathcal{W}_2(\mu, \mu^N) \quad (\text{By optimality of } \hat{T}^N) \\ &\leq \mathcal{W}_2(\hat{T}^\dagger \# \eta, \mu) + 2\mathcal{W}_2(\mu, \mu^N) \quad (\text{By the Triangle Inequality}) \\ &= \mathcal{W}_2(\hat{T}^\dagger \# \eta, T^\dagger \# \eta) + 2\mathcal{W}_2(\mu, \mu^N). \end{aligned}$$

By [\[6, Thm. 3.1\]](#) we have, for any pair of maps $T, T' \in L^2(\eta)$,

$$(3.5) \quad \mathcal{W}_2(T \# \eta, T' \# \eta) \leq \|T - T'\|_{L^2(\eta)},$$

and so the result follows by applying [\(3.5\)](#) to $\mathcal{W}_2(\hat{T}^\dagger \# \eta, T^\dagger \# \eta)$. ■

³Indeed practical generative models such as normalizing flows [\[36\]](#) are trained this way.

Remark 3.2. We note that [Theorem 3.1](#) is analogous to the oracle inequalities derived in [\[39\]](#). While the proof is simple, it has wide applications as it allows us to deal with the stochastic part of the error with the term $\mathcal{W}_2(\mu, \mu^N)$ which is a well-understood object in the empirical analysis of optimal transport. Indeed, such decompositions can be obtained for other metrics and divergences that satisfy a stability property, i.e., $\mathcal{D}(T\#\eta, T'\#\eta) \lesssim \|T - T'\|_{L^2(\eta)}$. However, the key to [Theorem 3.1](#) is that \widehat{T}^N is obtained by minimizing the same divergence \mathcal{D} that is also used for the error analysis. \diamond

It remains for us to bound $\mathcal{W}_2(\mu, \mu^N)$ to complete our error analysis. To this end, we recall the following well-known result on the empirical approximation of Wasserstein distances.

Lemma 3.3 ([\[19, Thm. 1\]](#)). *Suppose $\mu \in \mathbb{P}(\mathbb{R}^d)$ and $d > 4$ and that $\chi_q(\mu) := (\int_{\mathbb{R}^d} |u|^q \mu(du))^{1/q} < +\infty$ for some $q > 2$. Then there exists a constant $C > 0$, depending only on d , such that for all $N \geq 1$,*

$$\mathbb{E} \mathcal{W}_2^2(\mu, \mu^N) \leq C \chi_q^2(\mu) \left(N^{-2/d} - N^{-(q-2)/q} \right),$$

where the expectation is with respect to the empirical samples from μ .

Remark 3.4. Note that [\[19, Thm. 1\]](#) covers the case $d < 4$ but this mostly leads to unwieldy expressions for us that have little bearing on the main implications of our theory since $d > 4$ is reasonable for most practical inverse problems. In fact, henceforth we assume that $q > 2d/(d-2)$ so that the term $N^{-(q-2)/q}$ can be dropped and we have the simpler rate $N^{-2/d}$. \diamond

We are now ready to give our first error bound for generative priors.

Proposition 3.5. *Suppose $d > 4$, $\mu \in \mathbb{P}(\mathbb{R}^d)$, and $\chi_q(\mu) < +\infty$ for some $q > 2d/(d-2)$. Then there exists a constant $C > 0$, independent of N , such that for any $\epsilon > 0$ it holds with probability $1 - C\chi_q(\mu)N^{-1/d}/\epsilon$ that*

$$(3.6) \quad \mathcal{W}_2(\mu, \widehat{\mu}^N) \leq \|\widehat{T}^\dagger - T^\dagger\|_{L^2(\mu)} + \epsilon.$$

Proof. [Theorem 3.1](#) and [Theorem 3.3](#) together give

$$(3.7) \quad \mathbb{E} \mathcal{W}_2(\mu, \widehat{\mu}^N) \leq \|\widehat{T}^\dagger - T^\dagger\|_{L^2(\eta)} + C\chi_q(\mu)N^{-1/d}.$$

Absorbing the independent constants into C and applying Markov's inequality yields the result. \blacksquare

Remark 3.6. At this point one can directly work with [\(3.7\)](#) as opposed to the probabilistic statement [\(3.6\)](#). However, the latter becomes crucial when we analyze the error of posterior measures due to technicalities that arise in controlling the perturbation of the C_{stab} constants that appeared in [Subsection 3.2](#). \diamond

Following a similar approach for the proof of [Theorem 3.5](#) we can obtain a similar result for the case where the reference η is replaced with an empirical approximation η^M .

Lemma 3.7. *Suppose $T \in L^2(\eta)$ is globally Lipschitz with constant ℓ_T , then, for any pair of measures $\eta, \eta' \in \mathbb{P}(\mathcal{U})$ it holds that $\mathcal{W}_2(T\#\eta, T\#\eta') \leq \ell_T \mathcal{W}_2(\eta, \eta')$.*

Proof. Let π^* denote the optimal \mathcal{W}_2 coupling between η and η' . Then using the Lipschitz assumption on T we can write,

$$\begin{aligned} \mathcal{W}_2^2(T\#\eta, T\#\eta') &= \inf_{\pi \in \Pi(\eta, \eta')} \int_{\mathcal{U} \times \mathcal{U}} \|T(x) - T(y)\|_{\mathcal{U}}^2 \pi(\mathrm{d}x, \mathrm{d}y) \\ &\leq \int_{\mathcal{U} \times \mathcal{U}} \|T(x) - T(y)\|_{\mathcal{U}}^2 \pi^*(\mathrm{d}x, \mathrm{d}y) = \ell_T^2 \int_{\mathcal{U} \times \mathcal{U}} \|x - y\|_{\mathcal{U}}^2 \pi^*(\mathrm{d}x, \mathrm{d}y) \end{aligned}$$

■

Theorem 3.8. *Suppose $d > 4$, $\mu, \eta \in \mathbb{P}(\mathbb{R}^d)$, and $\chi_q(\mu), \chi_q(\eta) < +\infty$ for some $q > 2d/(d-2)$. Further suppose that the elements of $\widehat{\mathcal{T}}$ are uniformly globally Lipschitz with constant $\ell_{\widehat{\mathcal{T}}} > 0$. Then there exists a constant $C > 0$, independent of N and M , such that for any $\epsilon > 0$ it holds with probability $(1 - \ell_{\widehat{\mathcal{T}}} C \chi_q(\eta) M^{-1/d}/\epsilon)(1 - C \chi_q(\mu) N^{-1/d}/\epsilon)$ that*

$$\mathcal{W}_2(\mu, \widehat{\mu}^{M,N}) \leq \|\widehat{T}^\dagger - T^\dagger\|_{L^2(\eta)} + \epsilon.$$

Proof. Proceeding analogously to the proof of [Theorem 3.1](#) we can write

$$\begin{aligned} \mathcal{W}_2(\widehat{\mu}^{N,M}, \mu) &= \mathcal{W}_2(\widehat{T}^{N,M}\#\eta, \mu) \\ &\leq \mathcal{W}_2(\widehat{T}^{N,M}\#\eta, \widehat{T}^{N,M}\#\eta^M) + \mathcal{W}_2(\widehat{T}^{N,M}\#\eta^M, \mu) \quad (\text{By the Triangle Inequality}) \\ &\leq \ell_{\widehat{\mathcal{T}}}\mathcal{W}_2(\eta, \eta^M) + \mathcal{W}_2(\widehat{T}^{N,M}\#\eta^M, \mu^N) + \mathcal{W}_2(\mu^N, \mu) \\ &(\text{By the Triangle Inequality, } \text{Theorem 3.7}) \\ &\leq \ell_{\widehat{\mathcal{T}}}\mathcal{W}_2(\eta, \eta^M) + \mathcal{W}_2(\widehat{T}^\dagger\#\eta^M, \mu^N) + \mathcal{W}_2(\mu^N, \mu) \quad (\text{By optimality of } \widehat{T}^{N,M}) \\ &\leq \ell_{\widehat{\mathcal{T}}}\mathcal{W}_2(\eta, \eta^M) + \mathcal{W}_2(\widehat{T}^\dagger\#\eta^M, \widehat{T}^\dagger\#\eta) + \mathcal{W}_2(\widehat{T}^\dagger\#\eta, \mu^N) + \mathcal{W}_2(\mu^N, \mu) \\ &(\text{By the Triangle Inequality}) \\ &\leq 2\ell_{\widehat{\mathcal{T}}}\mathcal{W}_2(\eta, \eta^M) + \mathcal{W}_2(\widehat{T}^\dagger\#\eta, \mu) + 2\mathcal{W}_2(\mu^N, \mu) \\ &(\text{By the Triangle Inequality and applying } \text{Theorem 3.7} \text{ again}) \end{aligned}$$

The second term can be controlled by [\(3.5\)](#) while we can apply [Theorem 3.3](#) to the first and third terms and absorbing the Lipschitz constant to get,

$$\mathbb{E} \mathcal{W}_2(\eta, \eta^M) \leq C \chi_q(\eta) M^{-1/d} \quad \mathbb{E} \mathcal{W}_2(\mu^N, \mu) \leq C \chi_q(\mu) N^{-1/d},$$

Applying Markov's inequality to each term, we have that

$$2\ell_{\widehat{\mathcal{T}}}\mathcal{W}_2(\eta, \eta^M) + 2\mathcal{W}_2(\mu^N, \mu) < \epsilon$$

with probability $(1 - 4\ell_{\widehat{\mathcal{T}}} C \chi_q(\eta) M^{-1/d}/\epsilon)(1 - 2C \chi_q(\mu) N^{-1/d}/\epsilon)$. Absorbing the independent constants into C completes the proof. ■

Remark 3.9. We note that the uniform Lipschitz assumption on the approximation class $\widehat{\mathcal{T}}$ may appear restrictive but it is feasible in practical applications by, for example, weight clipping strategies or regularization for neural nets [\[64, 11\]](#). ◇

Remark 3.10. We note that the factor $\chi_q(\widehat{T}^\dagger \# \eta)$ is innocuous and can be approximated by $\chi_q(\mu)$ provided that \widehat{T}^\dagger is close to T^\dagger in $L^q(\eta)$. To be precise, we observe that

$$\chi_q^q(\widehat{T}^\dagger \# \eta) = \int_{\mathbb{R}^d} |u|^q \widehat{T}^\dagger \# \eta(du) = \int_{\mathbb{R}^d} |\widehat{T}^\dagger(u)|^q \eta(du) = \|\widehat{T}^\dagger\|_{L^q(\eta)}^q.$$

Similarly $\chi_q(\mu) = \|T^\dagger\|_{L^q(\eta)}$. Thus, $\chi_q(\widehat{T}^\dagger \# \eta) \leq \|\widehat{T}^\dagger - T^\dagger\|_{L^q(\eta)} + \chi_q(\mu)$. \diamond

3.2. Posterior bounds. Combining the error bounds of [Subsection 3.1](#) with the perturbation analysis of [Subsection 2.2](#) we can present high probability error bounds for the posteriors of generative priors. We first treat priors with bounded support in [Subsection 3.2.1](#) followed by the unbounded support case in [Subsection 3.2.2](#).

Throughout this section we consider the posterior measure

$$\frac{d\widehat{\nu}^{N,M}}{d\widehat{\mu}^{N,M}} = \frac{1}{Z^{N,M}(y)} \exp(-\Phi(u; y)), \quad Z^{N,M}(y) = \widehat{\mu}^{N,M}(\exp(-\Phi(u; y))),$$

as our approximation to the ground truth posterior ν from [\(1.1\)](#) with the prior approximated by a generative model with N samples from μ and M samples from η .

3.2.1. The bounded support case. In this section we assume that $\mathcal{U} \subset \mathbb{R}^d$ is a bounded set and the prior $\widehat{\mu}$ and its approximation $\widehat{\mu}^{M,N}$ are both supported on \mathcal{U} . We begin with a lemma for controlling the stability constant C_{stab} from [Theorem 2.2](#) and [Theorem 2.3](#).

Lemma 3.11. *Suppose \mathcal{U} is bounded, $\mu, \widehat{\mu} \in \mathbb{P}^2(\mathcal{U})$ and $\Phi \in \mathcal{F}(f, g, h, \ell, \mu)$ such that $(1 + \|\cdot\|_{\mathcal{U}})f \in L^1(\mu)$ and $h(\cdot, y)$ is globally $\ell_h(y)$ -Lipschitz, i.e.,*

$$|h(u, y) - h(u', y)| \leq \ell_h(y) \|u - u'\|_{\mathcal{U}}.$$

Further suppose $\mathcal{W}_2(\mu, \widehat{\mu}) < \epsilon$ for a small constant $\epsilon > 0$. Then it holds that

$$(3.8) \quad C_{\text{stab}}(y) \leq \left[\frac{g^2(y) \|(1 + \|\cdot\|_{\mathcal{U}})f\|_{L^1(\mu)}}{\|h(\cdot, y)\|_{L^1(\mu)} (\|h(\cdot, y)\|_{L^1(\mu)} - \ell_h(y)\epsilon)} \right] \times [1 \vee \text{Diam}(\mathcal{U})] \left(\int_{\mathcal{U} \times \mathcal{U}} [1 \vee \ell(u, v, y)]^2 \cdot [f(u) \vee f(v)]^2 \pi^*(du, dv) \right)^{\frac{1}{2}},$$

where $\text{Diam}(\mathcal{U}) = \sup_{u, u' \in \mathcal{U}} \|u - u'\|_{\mathcal{U}}$ is the diameter of \mathcal{U} .

Proof. Since \mathcal{U} is bounded we can write

$$(3.9) \quad \begin{aligned} & \left(\int_{\mathcal{U} \times \mathcal{U}} [1 \vee \ell(u, v, y)]^2 \cdot [f(u) \vee f(v)]^2 \cdot [1 \vee \|u\|_{\mathcal{U}} \vee \|v\|_{\mathcal{U}}]^2 \pi^*(du, dv) \right)^{\frac{1}{2}}, \\ & \leq \left([1 \vee \text{Diam}(\mathcal{U})]^2 \int_{\mathcal{U} \times \mathcal{U}} [1 \vee \ell(u, v, y)]^2 \cdot [f(u) \vee f(v)]^2 \cdot \pi^*(du, dv) \right)^{\frac{1}{2}}, \\ & = [1 \vee \text{Diam}(\mathcal{U})] \left(\int_{\mathcal{U} \times \mathcal{U}} [1 \vee \ell(u, v, y)]^2 \cdot [f(u) \vee f(v)]^2 \cdot \pi^*(du, dv) \right)^{\frac{1}{2}}. \end{aligned}$$

Now let π^{**} be the optimal \mathcal{W}_1 coupling between μ and $\widehat{\mu}$ and integrate both sides of the Lipschitz condition $h(u, y) - h(u', y) \leq \ell_h(y)\|u - u'\|_{\mathcal{U}}$ with respect to this coupling to obtain

$$\mu(h(\cdot, y)) - \widehat{\mu}(h(\cdot, y)) \leq \ell_h(y)\mathcal{W}_1(\mu, \widehat{\mu}).$$

But h is non-negative and so $\mu(h(\cdot, y)) = \|h(\cdot, y)\|_{L^1(\mu)}$ and similarly $\widehat{\mu}(h(\cdot, y)) = \|h(\cdot, y)\|_{L^1(\widehat{\mu})}$. Furthermore, $\mathcal{W}_1(\mu, \widehat{\mu}) \leq \mathcal{W}_2(\mu, \widehat{\mu})$ (see for example [63, Rem. 6.6]), and so we obtain the lower bound $\|h(\cdot, y)\|_{L^1(\mu)} - \ell_h(y)\epsilon \leq \|h(\cdot, y)\|_{L^1(\widehat{\mu})}$. Substituting this bound alongside (3.9) into (2.6) completes the proof. \blacksquare

We need a second technical lemma that is useful in the proof of our main theorem below.

Lemma 3.12. *Suppose $\varphi : \mathcal{U} \times \mathcal{U} \rightarrow \mathbb{R}$ is ℓ_φ -Lipschitz with respect to the metric $\varrho((u, v), (u', v')) := \|u - u'\|_{\mathcal{U}} + \|v - v'\|_{\mathcal{U}}$, i.e.,*

$$|\varphi(u, v) - \varphi(u', v')| \leq \ell_\varphi (\|u - u'\|_{\mathcal{U}} + \|v - v'\|_{\mathcal{U}}).$$

Suppose $\mu, \widehat{\mu} \in \mathbb{P}(\mathcal{U})$ such that $\mathcal{W}_2(\mu, \widehat{\mu}) < \epsilon$ and let π^ denote the corresponding optimal \mathcal{W}_2 coupling. Then it holds that*

$$\left| \int_{\mathcal{U}} \varphi(u, u) \mu(du) - \int_{\mathcal{U} \times \mathcal{U}} \varphi(u, v) \pi^*(du, dv) \right| \leq \ell_\varphi \epsilon.$$

Proof. By the Lipschitz assumption on φ and Cauchy-Schwarz we have that

$$\begin{aligned} \left| \int_{\mathcal{U}} \varphi(u, u) \mu(du) - \int_{\mathcal{U} \times \mathcal{U}} \varphi(u, v) \pi^*(du, dv) \right| &\leq \int_{\mathcal{U} \times \mathcal{U}} |\varphi(u, u) - \varphi(u, v)| \pi^*(du, dv) \\ &\leq \ell_\varphi \int_{\mathcal{U} \times \mathcal{U}} \|u - v\|_{\mathcal{U}} \pi^*(du, dv) \\ &\leq \ell_\varphi \left(\int_{\mathcal{U} \times \mathcal{U}} \|u - v\|_{\mathcal{U}}^2 \pi^*(du, dv) \right)^{1/2} = \ell_\varphi \epsilon. \end{aligned}$$

We are now ready to combine Theorem 3.11 with Theorem 2.2 and Theorem 3.8 to obtain our first quantitative error bound for the posteriors.

Theorem 3.13. *Suppose Theorem 3.8, and Theorem 3.11 are satisfied and define the function*

$$(3.10) \quad \varphi(u, v, y) := (1 + \ell(u, v, y)^2)(f(u)^2 + f(v)^2).$$

Suppose $\varphi(\cdot, \cdot, y)$ is $\ell_\varphi(y)$ -Lipschitz with respect to the metric

$$(3.11) \quad \varrho((u, v), (u', v')) = \|u - u'\|_{\mathcal{U}} + \|v - v'\|_{\mathcal{U}}.$$

Then there exists an independent constant $C > 0$ so that for any $\epsilon > 0$, with probability $(1 - \ell_{\widehat{T}} C \chi_q(\eta) M^{-1/d}/\epsilon)(1 - C \chi_q(\mu) N^{-1/d}/\epsilon)$, it holds that

$$\mathcal{W}_1(\widehat{\nu}^{N, M}, \nu) \leq C'_{\text{stab}}(y)[1 \vee \text{Diam}(\mathcal{U})] \left(\|\widehat{T}^\dagger - T^\dagger\|_{L^2(\eta)} + \epsilon \right),$$

where $C'_{\text{stab}}(y) > 0$ has the expression

$$C'_{\text{stab}}(y) = \frac{g^2(y) (\|(1 + \|\cdot\|_{\mathcal{U}})f\|_{L^1(\mu)}) (2\|\varphi(\cdot, \cdot, y)\|_{L^1(\mu)} + \ell_{\varphi}(y)\epsilon)^{1/2}}{\|h(\cdot, y)\|_{L^1(\mu)} (\|h(\cdot, y)\|_{L^1(\mu)} - \ell_h(y)\epsilon)}.$$

Proof. Suppose [Theorem 3.8](#) holds and consider the event $\mathcal{W}_2(\mu, \hat{\mu}^{N,M}) < \epsilon$. Then by [Theorem 3.11](#) we have that

$$\mathcal{W}_1(\hat{\nu}^{N,M}, \nu) \leq C(y) \frac{\|\hat{T}^{\dagger} - T^{\dagger}\|_{L^2(\eta)} + \epsilon}{\|h(\cdot, y)\|_{L^1(\mu)} (\|h(\cdot, y)\|_{L^1(\mu)} - \ell_h(y)\epsilon)}$$

where we have

$$\begin{aligned} C(y) &= g^2(y) (\|f\|_{L^1(\mu)} + \|f \cdot \|\cdot\|_{\mathcal{U}}\|_{L^1(\mu)}) \\ &\times [1 \vee \text{Diam}(\mathcal{U})] \left(\int_{\mathcal{U} \times \mathcal{U}} [1 \vee \ell(u, v, y)]^2 \cdot [f(u) \vee f(v)]^2 \pi^*(du, dv) \right)^{1/2}. \end{aligned}$$

Note that the integral in the second line still depends on $\hat{\mu}^{N,M}$ due to the optimal coupling $\pi^* \in \Pi(\mu, \hat{\mu}^{N,M})$ and so we need to control the fluctuations of this term. Applying [Theorem 3.12](#) with the function $\varphi(u, v, y) = (1 + \ell(u, v, y)^2)(f(u)^2 + f(v)^2)$, and thanks to the hypothesis of the theorem, gives

$$\int_{\mathcal{U} \times \mathcal{U}} [1 \vee \ell(u, v, y)]^2 \cdot [f(u) \vee f(v)]^2 \pi^*(du, dv) \leq 2 \int_{\mathcal{U}} (1 + \ell^2(u, u, y)) f^2(u) \mu(du) + \ell_{\varphi}(y)\epsilon.$$

Substituting this bound into the expression for $C(y)$ completes the proof. \blacksquare

Remark 3.14. Assuming both ϵ and $\|\hat{T}^{\dagger} - T^{\dagger}\|_{L^2(\eta)}$ are small and ignoring higher order terms, this theorem simply states that the posterior error is controlled by the approximation error of \hat{T}^{\dagger} and ϵ itself which quantifies the stochastic error due to the empirical approximation of the prior. The multiplying constant $C'_{\text{stab}}(y)$ in the bound, although complex in its expression, is effectively controlled by generalized moments of the prior μ and hence can be bounded so long as μ has sufficiently light tails. \diamond

Remark 3.15. Note that the reason why we considered \mathcal{U} to be bounded in this section is largely due to the $\|h(\cdot, y)\|_{L^1(\hat{\mu})}$ factor in [\(2.6\)](#) since this quantity is random when $\hat{\mu} = \hat{\mu}^{N,M}$. When \mathcal{U} is bounded any Lipschitz h is automatically globally Lipschitz which allows us to control the variation of $\|h(\cdot, y)\|_{L^1(\mu)} - \|h(\cdot, y)\|_{L^1(\hat{\mu}^{N,M})}$. Hence our proof in this section can naturally be extended to the case of a globally Lipschitz h with unbounded \mathcal{U} . \diamond

Remark 3.16. We note that the dependence of C'_{stab} on the data y is explicit through the functions h and φ and their Lipschitz constants. This provides a path for further obtain high-probability bounds on posterior perturbations with respect to the data y as well as the empirical data. This requires detailed calculations using the explicit forms of h and φ , for specific examples which we leave as a future research direction. \diamond

Remark 3.17. We note that our bounds can be simplified whenever the functions ℓ and f are bounded. For example, suppose that

$$\ell(u, v, y) \leq \ell_{\max}(y) < +\infty \quad \text{and} \quad f(u) \leq f_{\max} < +\infty \quad \text{for all } u, v \in \mathcal{U}.$$

In this case, we can drop the assumptions on the function φ in [Theorem 3.13](#) and directly bound the constant $C_{\text{stab}}(y)$ in [\(3.8\)](#) as

$$C_{\text{stab}}(y) \leq \frac{g^2(y) f_{\max}^2 \|1 + \|\cdot\|_{\mathcal{U}}\|_{L^1(\mu)}}{\|h(\cdot, y)\|_{L^1(\mu)} (\|h(\cdot, y)\|_{L^1(\mu)} - \ell_h(y)\epsilon)} [1 \vee \text{Diam}(\mathcal{U})] [1 \vee \ell_{\max}(y)],$$

which allows us to obtain an equivalent version of [Theorem 3.13](#) with a cleaner constant C_{stab} but essentially the same rate in terms of the parameter ϵ and the approximation error $\|\hat{T}^\dagger - T^\dagger\|_{L^2(\eta)}$. The same bound can also be extended to the unbounded support case described in the next section with the exception that we will assume that $\ell(\cdot, \cdot, y)$ and f are only locally bounded over \mathcal{U} . \diamond

3.2.2. The unbounded support case. Let us now turn our attention to the case where \mathcal{U} is unbounded and hence μ may have unbounded support. We will deal with this case by truncating the prior to a ball of radius r and applying our bounded support result with an additional error term due to the trimming of the tails. To this end, define the trimmed prior

$$\mu_r(A) := \frac{1}{\mu(B_r)} \mu(A \cap B_r)$$

for all Borel sets $A \subseteq \mathcal{U}$ and B_r denoting the ball of radius $r > 0$ in \mathcal{U} . Further define the trimmed posterior

$$\frac{d\nu_r}{d\mu_r} = \frac{1}{Z_r(y)} \exp(-\Phi(u; y)), \quad Z_r(y) := \mu_r(\exp(-\Phi(\cdot; y))).$$

We then have the following lemma, quantifying the effect of trimming the prior tails.

Lemma 3.18. *Consider the above setup, we then have the bounds⁴*

$$\mathcal{W}_1(\nu, \nu_r) \leq \frac{2}{r} \nu(\|\cdot\|_{\mathcal{U}})^2, \quad \mathcal{W}_2(\mu, \mu_r) \leq \frac{2}{r} \mu(\|\cdot\|_{\mathcal{U}}^2).$$

Proof. Let us begin with the posterior \mathcal{W}_1 bound. Define the measure

$$\nu_r^c(A) := \frac{1}{\nu(B_r^c)} \nu(A \cap B_r^c)$$

where B_r^c is the complement of B_r in \mathcal{U} . Then consider the coupling $\pi_1 \in \Pi(\nu, \nu_r)$ where $(u, u') \sim \pi_1$ are generated by the following procedure

$$\text{draw } u \sim \nu \text{ if } \|u\|_{\mathcal{U}} \leq r, \text{ set } u' = u, \text{ else, draw } u' \sim \nu_r.$$

⁴Indeed, the fact that μ and ν are prior and posterior measures is innocuous in this lemma and the bounds apply to any measure and its corresponding trimmed version. We simply state them this way for easier use later.

Then by the definition of \mathcal{W}_1 we have that

$$\begin{aligned} \mathcal{W}_1(\nu, \nu_r) &\leq \int_{\mathcal{U} \times \mathcal{U}} \|u - u'\|_{\mathcal{U}} \pi_1(du, du') \\ &= \int_{\{u \in B_r^c\}} \int_{\mathcal{U}} \|u - u'\|_{\mathcal{U}} \pi_1(du' | u) \pi_1(du) + \int_{\{u \in B_r^c\}} \int_{\mathcal{U}} \|u - u'\|_{\mathcal{U}} \pi_1(du' | u) \pi_1(du). \end{aligned}$$

The first term is zero by construction while for the second term we have the bound

$$\begin{aligned} \int_{\{u \in B_r^c\}} \int_{\mathcal{U}} \|u - u'\|_{\mathcal{U}} \pi_1(du' | u) \pi_1(du) &\leq \int_{\{u \in B_r^c\}} \int_{\mathcal{U}} \|u\|_{\mathcal{U}} + \|u'\|_{\mathcal{U}} \pi_1(du' | u) \pi_1(du) \\ &\leq 2\nu(\mathcal{U} \cap B_r^c) \nu(\|\cdot\|_{\mathcal{U}}), \end{aligned}$$

where in the last inequality we used the fact that $\|u\|_{\mathcal{U}} \geq \|u'\|_{\mathcal{U}}$ a.s. under π_1 . An application of Markov's inequality yields $\nu(\mathcal{U} \cap B_r^c) \leq \frac{\nu(\|\cdot\|_{\mathcal{U}})}{r}$ which completes the proof of the \mathcal{W}_1 bound for priors.

We can apply the same proof technique to the posteriors, writing $\pi_0 \in \Pi(\mu, \mu_r)$ for the analogous coupling obtained by replacing ν, ν_r with μ, μ_r in the definition of π_1 . Then we obtain the bound

$$\mathcal{W}_2^2(\mu, \mu_r) \leq 2 \int_{\{u \in B_r^c\}} \int_{\mathcal{U}} \|u\|_{\mathcal{U}}^2 + \|u'\|_{\mathcal{U}}^2 \pi_0(du' | u) \pi_0(du) \leq 4\mu(\mathcal{U} \cap B_r^c) \mu(\|\cdot\|_{\mathcal{U}}^2),$$

where the extra factor of 2 is due to $(a + b)^2 \leq 2(a^2 + b^2)$. Applying Markov's inequality we have $\mu(\mathcal{U} \cap B_r^c) \leq \frac{\mu(\|\cdot\|_{\mathcal{U}}^2)}{r^2}$ which completes the proof. \blacksquare

Equipped with the above lemma we are finally ready to present our complete error bound for the case of unbounded parameter spaces \mathcal{U} .

Theorem 3.19. *Suppose $d > 4$, \mathcal{U} is unbounded, and fix $r \geq 1$. Consider the trimmed generative prior model*

$$\hat{\mu}_r^{N,M} := \hat{T}_r^{N,M} \# \eta \quad \hat{T}_r^{N,M} := \arg \min_{T \in \hat{\mathcal{T}}} \mathcal{W}_1(T \# \eta^M, \mu_r^N).$$

where the approximation class $\hat{\mathcal{T}}$ is globally $\ell_{\hat{\mathcal{T}}}$ -Lipschitz. Further write $\hat{\nu}_r^{N,M}$ for the posterior measure arising from $\hat{\mu}_r^{N,M}$. Write T_r^\dagger for the map that satisfies $\mu_r = T_r^\dagger \# \eta$ and define $\hat{T}_r^\dagger := \arg \min_{T \in \hat{\mathcal{T}}} \|T - T_r^\dagger\|_{L^2(\eta)}$, $\hat{T}_r^* := \arg \max_{T \in \hat{\mathcal{T}}} \mathcal{W}_2(T \# \eta, T \# \eta^M)$.

Suppose the following conditions hold:

- (i) $\Phi \in \mathcal{F}(f, g, h, \ell, \mu)$ such that $(1 + \|\cdot\|_{\mathcal{U}})f \in L^1(\mu_r)$.
- (ii) The function $h(\cdot, y)$ is $\ell_{h,r}(y)$ -Lipschitz over $\mathcal{U} \cap B_r$.
- (iii) The function $\varphi(\cdot, \cdot, y)$ defined in (3.10) is $\ell_{\varphi,r}(y)$ -Lipschitz with respect to the metric ϱ defined in (3.11) over $(\mathcal{U} \cap B_r) \times (\mathcal{U} \cap B_r)$.
- (iv) $\chi_q(\mu), \chi_q(\eta) < +\infty$ for some $q > 2d/(d-2)$.

Then there exists a constant $C > 0$ so that for any $\epsilon > 0$, with probability $(1 -$

$\ell_{\widehat{\tau}} C_{\chi_q}(\eta) M^{-1/d}/\epsilon)(1 - C_{\chi_q}(\mu) N^{-1/d}/\epsilon)$, it holds that

$$\mathcal{W}_1(\widehat{\nu}_r^{N,M}, \nu) \leq C_{\text{stab}}(y, r) \cdot (\|\widehat{T}_r^\dagger - T^\dagger\|_{L^2(\eta)} + \epsilon) + \frac{2}{r} \nu(\|\cdot\|_{\mathcal{U}})^2,$$

where $C'_{\text{stab}}(y, r)$ has the expression

$$C_{\text{stab}}(y, r) = \frac{2g^2(y) (\|(1 + \|\cdot\|_{\mathcal{U}})f\|_{L^1(\mu_r)}) (2\|\varphi(\cdot, \cdot, y)\|_{L^1(\mu_r)} + \ell_{\varphi, r}(y)\epsilon)^{1/2} r}{\|h(\cdot, y)\|_{L^1(\mu_r)} (\|h(\cdot, y)\|_{L^1(\mu_r)} - \ell_{h, r}(y)\epsilon)}.$$

Proof. By the triangle inequality we have $\mathcal{W}_1(\widehat{\nu}_r^{N,M}, \nu) \leq \mathcal{W}_1(\widehat{\nu}_r^{N,M}, \nu_r) + \mathcal{W}_1(\nu_r, \nu)$. We can bound the second term using [Theorem 3.18](#) while the first term is bounded using [Theorem 3.13](#) by replacing μ with μ_r and observing $\text{Diam}(\mathcal{U}) \leq 2r$. \blacksquare

Remark 3.20. Observe that the posterior moment $\nu(\|\cdot\|_{\mathcal{U}})$ can further be controlled by the prior moment $\mu(\|\cdot\|_{\mathcal{U}})$ using our assumptions on the likelihood potential Φ , i.e., by Cauchy-Schwarz we have

$$\nu(\|\cdot\|_{\mathcal{U}}) \leq \frac{1}{Z(y)} \mu(\|\cdot\|_{\mathcal{U}}^2)^{1/2} (g(y) + \|f\|_{L^2(\mu)}).$$

Since $Z(y) \geq \|h(\cdot, y)\|_{L^1(\mu)}$ we can further obtain the bound

$$\nu(\|\cdot\|_{\mathcal{U}})^2 \leq \frac{(g(y) + \|f\|_{L^2(\mu)})^2 \mu(\|\cdot\|_{\mathcal{U}}^2)}{\|h(\cdot, y)\|_{L^1(\mu)}^2}.$$

This reveals that the posterior error due to trimming, has the same detrimental scaling due to the evidence $Z(y)$ or similarly $\|h(\cdot, y)\|_{L^1(\mu)}$ as the constant C_{stab} and so the entire bound becomes innocuous when the data y is "unlikely" in the sense of having very small evidence $Z(y)$. This is a well-known phenomenon that was observed in [\[56\]](#) and highlights the mechanism underpinning the brittleness of BIPs in [\[49\]](#). \diamond

4. Numerical Results. In this section we collect a series of numerical experiments aimed at verifying some of our error bounds. In particular, we focus on the posterior perturbation bounds in terms of the priors from [Section 2](#). In [Subsection 4.1](#) we present a series of 2D benchmarks where we explicitly check that the posterior \mathcal{W}_1 distance is controlled by the prior \mathcal{W}_2 distance. In [Subsection 4.2](#) we present an example of a nonlinear PDE inverse problem with a generative prior and demonstrate the effectiveness of generative priors for more complex and realistic examples. Our code to reproduce the numerical results can be found in a public Github repository⁵.

4.1. 2D Benchmarks. We begin with a set of low dimensional benchmarks where posterior samples can be generated accurately and cheaply using importance sampling. This allows us to compute precise Wasserstein distances between true posteriors and those with a generative prior without additional noise due to posterior inference algorithms such as MCMC that can often pollute our results.

⁵<https://github.com/TADSGroup/DataDrivenBIPwithGenerativePrior/tree/main>

Problem setup. We took $\mathcal{U} = \mathbb{R}^2$ and took our prior measures μ to be the benchmark distributions taken from [35]; these are depicted in Figure 4.1. Here we present the Swissroll, Pinwheel, and Checkerboard distributions since we found these to be good representatives of our findings. We found very similar results for the other benchmarks from [35].

To define the posterior measures ν we considered the likelihood potential

$$\Phi(u; y) = \frac{1}{2\sigma^2} \|y - Fu\|_2^2, \quad F = \begin{bmatrix} 1 & 0 \\ 0 & 0 \end{bmatrix}.$$

This likelihood arises from the familiar data model $y = Fu + \xi$ where the additive noise $\xi \sim N(0, \sigma^2 I)$. Here we chose $\sigma = 0.5$. The resulting posteriors are depicted in Figure 4.1 for a fixed choice of the data $y = (0, 0)^T$. The presented heatmaps were obtained by generating prior samples that were reweighted and resampled according to their likelihoods. We took these to be samples from the true posterior measures ν in our experiments.

The generative prior. We used a Wasserstein GAN with gradient penalty (WGAN-gp) [23] as a generative approximation to the priors above and computing the maps \hat{T} and in turn the priors $\hat{\mu}$. In general, we found the WGAN-gps to be difficult to train in order to obtain highly accurate approximations to the priors, to this end, we modified the training procedure by borrowing ideas from stochastic interpolants [3]; the details are summarized in Section A. With a generative prior at hand, we can use the same reweighting trick as the true posterior to obtain samples from the approximate posteriors $\hat{\nu}$. In Figure 4.1 we show an instance of the learned priors and the resulting posteriors.

Experiments and results. Our goal was to investigate the validity of the perturbation bounds of Section 2 and in particular Theorem 2.2. To this end, we compared the $\mathcal{W}_1(\nu, \hat{\nu})$ and compared it with $\mathcal{W}_2(\mu, \hat{\mu})$ for various generative priors $\hat{\mu}$ by varying the size of the training data for the GAN as well as the size of the networks. In particular, we considered the following scenarios:

- *Effect of the sample size N :* We fixed our WGAN-gp architecture and training procedure (see Section A) and increased the number of prior training samples N from 2^9 to 2^{14} .
- *Effect of network width:* We fixed the number of training samples $N = 10000$ and used a generator with three layers but we modified the width of the layers from 2^4 to 2^8 . The number training epochs and the discriminator architectures were kept fixed.
- *Effect of training epochs:* Finally, we considered a fixed $N = 10000$ and a network of depth 3 and width 128 and increased the number of training epochs from 2^8 to 2^{12} . Once again the discriminator architectures were kept fixed.

We think of the first experiment (modifying N) as representing the stochastic training errors while the other experiments reflect the approximation bias/error of our parameterizations.

We present our results in Figures 4.2 to 4.4 where the prior \mathcal{W}_2 distances are compared with the posterior \mathcal{W}_1 distances as a function of the underlying variables. We repeated each experiments 5 times and presented the average errors along with the error bars obtained from repeated experiments. We consistently observed that the posterior \mathcal{W}_1 distance was controlled by the prior \mathcal{W}_2 distances with the underlying slopes matching closely as shown in Table 4.1. We take this as a validation of our bound in Theorem 2.2. Interestingly, we observed that

the prior \mathcal{W}_2 slopes (and by extension the posterior slopes) did not match the empirical $N^{-1/2}$ rate predicted by [19]. We take this as evidence that WGAN-gp is not a good estimator of the prior in the \mathcal{W}_2 sense.

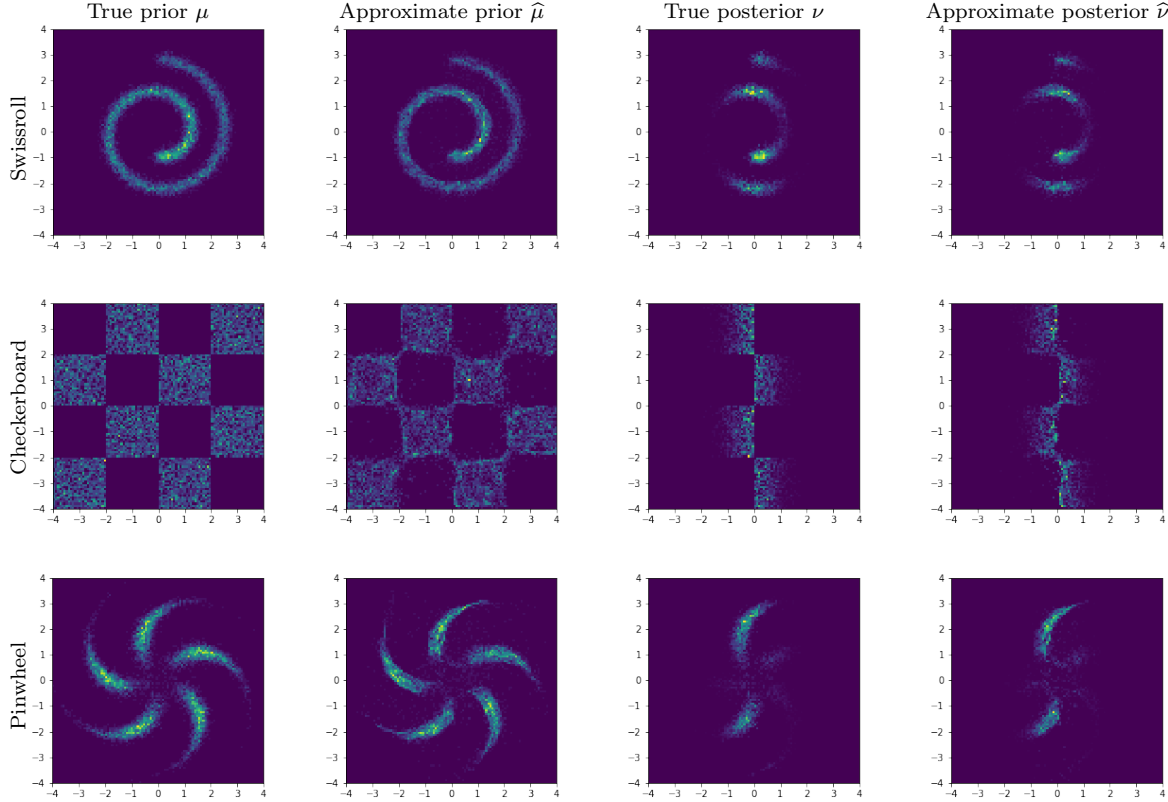


Figure 4.1: Example of 2D Benchmarks from [Subsection 4.1](#) with three example distributions. From left to right, the first column depicts the true prior μ , the second column shows the data-driven prior $\hat{\mu}$, the third column shows the true posterior samples ν , while the fourth column shows samples from the data-driven posterior $\hat{\nu}$. The heatmaps for the posterior were generated by reweighting the prior samples using the likelihood.

4.2. A PDE Example. We now consider a PDE inverse problem as an instance of a high-dimensional problem, in order to demonstrate the effectiveness of generative priors for solving inverse problems in scientific computing. The problem considered here is synthetic and designed specifically to demonstrate the efficacy of data-driven BIPs in handling complex and multi-modal priors and posteriors arising from PDEs and using simple sampling algorithms. We also note that while our analysis in the rest of the paper was tailored to finite dimensional parameters, i.e., we always assumed $\mathcal{U} \subseteq \mathbb{R}^d$, in this example the parameter is truly infinite dimensional although we work with a discretization of the problem. However, we use dimension reduction techniques alongside function space MCMC algorithms to ensure the resulting

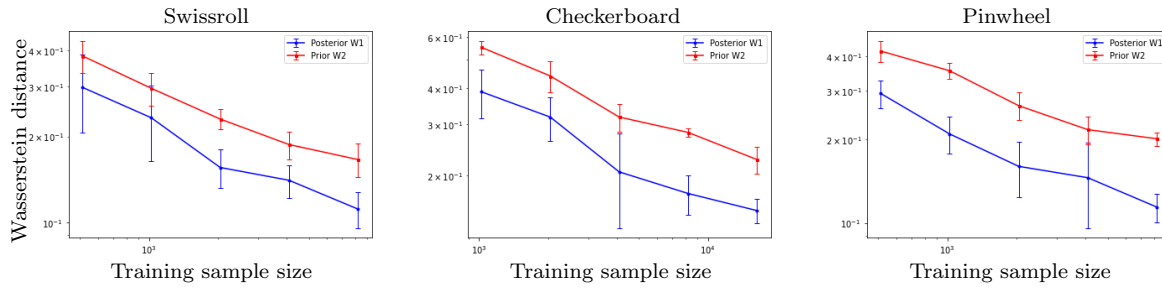


Figure 4.2: Comparing the convergence of data-driven priors in the \mathcal{W}_2 metric versus the subsequent posteriors in the \mathcal{W}_1 metric as a function of the training sample size for the 2D benchmarks from Subsection 4.1. In all cases the prior \mathcal{W}_2 distance controls the posterior \mathcal{W}_1 distance. Slopes of linear fits to these curves, indicating rate of convergence with the sample size, are reported in Table 4.1.

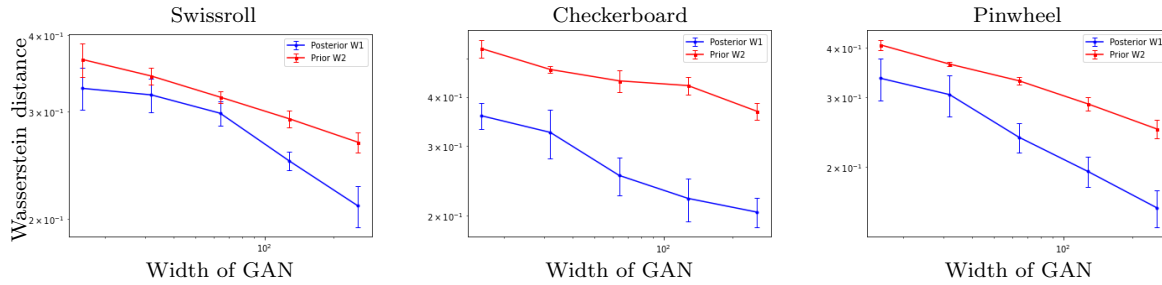


Figure 4.3: Comparing the convergence of data-driven priors in the \mathcal{W}_2 metric versus the subsequent posteriors in the \mathcal{W}_1 metric as a function of the width of the generator for the 2D benchmarks from Subsection 4.1. In all cases the prior \mathcal{W}_2 distance controls the posterior \mathcal{W}_1 distance. Slopes of linear fits to these curves, indicating rate of convergence with width of the generator, are reported in Table 4.1.

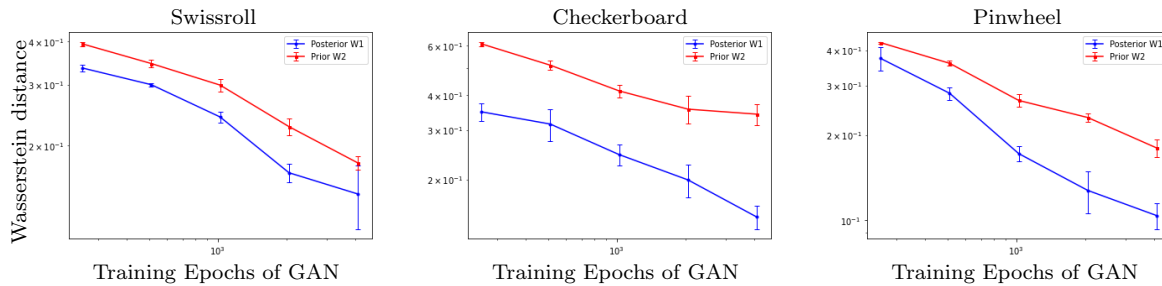


Figure 4.4: Comparing the convergence of data-driven priors in the \mathcal{W}_2 metric versus the subsequent posteriors in the \mathcal{W}_1 metric as a function of the number of training epochs for the 2D benchmarks from Subsection 4.1. In all cases the prior \mathcal{W}_2 distance controls the posterior \mathcal{W}_1 distance. Slopes of linear fits to these curves, indicating rate of convergence with the number of training epochs, are reported in Table 4.1.

	Training sample size		Network width		Training epochs	
	Prior \mathcal{W}_2	Post. \mathcal{W}_1	Prior \mathcal{W}_2	Post. \mathcal{W}_1	Prior \mathcal{W}_2	Post. \mathcal{W}_1
Swissroll	-0.307	-0.357	-0.113	-0.164	-0.289	-0.327
Checkerboard	-0.321	-0.359	-0.119	-0.218	-0.219	-0.316
Pinwheel	-0.281	-0.325	-0.174	-0.282	-0.312	-0.485

Table 4.1: We report the slopes of linear fits, in the log-log scale, of the W_1 distance of data-driven posteriors compared to the ground truth alongside the W_2 distance of data-driven priors. In both cases we report the errors as a function of the sample size of the training data, width of WGAN-gp, and number of training epochs. The left two columns correspond to the plots in Figure 4.2, the third and fourth columns correspond to the plots in Figure 4.3, while the two columns on the right correspond to Figure 4.4.

methodology is mesh independent.

Problem Setup. We consider the Darcy flow PDE which is a simple model of the flow of a fluid in a porous medium:

$$\begin{cases} -\operatorname{div}(\exp(u(x))\nabla p(x)) = f(x), & x \in (0, 1)^2, \\ p(x) = 0, & x \in \partial(0, 1)^2. \end{cases}$$

where u is the log of the permeability field and p denotes the pressure. The inverse problem of interest is that of estimating the permeability field $\exp(u)$ from pointwise measurements of the pressure p . To this end, we define the likelihood

$$\Phi(u; y) = \frac{1}{2\sigma^2} \|y - F(u)\|_2^2,$$

where $F : u \rightarrow (p(x_1) \dots p(x_{300})) \in \mathbb{R}^{300}$ with the x_i denoting a fixed collection of observation points in the domain; see Figure 4.5. Hence, the forward map F consists of the composition of the parameter-to-solution map of the PDE with a pointwise evaluation map. We approximate this map by solving the PDE using finite elements. To make the problem interesting we assume that the prior on u is the distribution of the MNIST data set. Since the map F is smoothing and loses a lot of information about u we expect that a generative model trained on MNIST should give rise to a multi-modal posterior since many choices of u can generate the observed data.

The generative prior. We discretized $\mathcal{U} = \mathbb{R}^{784}$ viewing MNIST images as piecewise constant functions⁶ and trained a WGAN-gp on the MNIST data set as our generative prior; see Section B for details.

Posterior sampling in the latent space. Since our problem is high dimensional we can no longer use the likelihood to re-weight the prior samples as in the 2D benchmarks in Subsection 4.1. Instead, we employ the preconditioned-Crank-Nicolson (pCN) algorithm of [13] in the latent space of the GAN. To be precise, let $\hat{T} : z \mapsto u$ denote our GAN, transforming i.i.d.

⁶We can also work with a PCA dimension reduction to ensure that the formulation is discretization invariant.

Gaussian noise η to the MNIST image space. We then consider the inverse problem

$$\frac{d\hat{\gamma}}{d\eta}(z) = \frac{1}{Z(y)} \exp\left(-\Phi(\hat{T}(z); y)\right), \quad Z(y) = \eta(\exp(-\Phi(T(z); y))),$$

where γ now denotes the posterior on the latent variable z and we slightly abused notation to indicate the normalizing constant as $Z(y)$ as before. The data-driven posterior is simply given by $\hat{T}\#\hat{\gamma}$. In other words, if we use pCN to generate posterior samples in the latent space we can then push those samples through the GAN to obtain samples from the target posterior $\hat{\nu}$ supported on the image space. We note that the articles [51, 9] used a similar approach for posterior sampling. The resulting procedure is summarized in [Algorithm 4.1](#).

Experiments and results. We considered two experiments using the same set of observation points with the true parameter u chosen as an image of the digit "3" as shown in [Figure 4.5\(a\)](#). We considered two choices of σ arising from 10% and 20% noise-to-signal ratio.

[Figure 4.5](#) summarizes our results in the high noise regime (20% noise-to-signal ratio) using 2×10^5 MCMC samples. We observed that the posterior mean did not match the correct digit and the posterior variance was high. Indeed, the posterior is multimodal as shown in [Figure 4.6](#) where we can see that the digits "3, 8, 2, 5" appear in posterior samples. This is precisely the behavior we aimed to capture with our method since simple MCMC algorithms such as pCN often struggle to traverse the support of multi-model posteriors. However, using pCN in the latent space of the GAN appears to resolve this issue in our example. [Figure 4.7\(d\)](#) and (e) show coordinate-wise autocorrelation functions and effective sample sizes of pCN, indicating good performance and mixing of the algorithm.

[Figure 4.7](#) shows the results of our experiment in the low noise regime with noise-to-signal ratio of 10% using 10^6 MCMC samples. As expected, the MCMC chain converges slower in the low noise regime due to the concentration of the prior. We show the same quantities as in the previous experiment. We see that the posterior mean is now a close match to the original image and appears to be unimodal based on the independent samples shown in [Figure 4.8](#). We believe that in this instance the observed data is of high enough quality that allows us to recover a close approximation to the true image.

5. Conclusion. We developed a theoretical analysis of data-driven BIPs with generative priors learned from an empirical data. We considered a transport model for our generator and combined ideas from the perturbation analysis of BIPs with novel error analysis for minimum Wasserstein generative models to obtain quantitative error bounds for data-driven posteriors with respect to a ground truth posterior defined in the large data limit of the data-driven prior. Our analysis revealed a simple bias-variance trade-off, with an approximation bias coming from our parameterization of the generator and a stochastic error coming from the finite training data. However, the details of the analysis require various technical assumptions on the smoothness of the likelihood functions as well as tail properties of the prior. We further presented numerical experiments that verified the validity of some of our bounds in low-dimensional benchmarks where exact sampling of highly multi-modal posteriors was possible.

Our results lead to multiple follow up questions: (i) we primarily considered finite dimensional parameter spaces but most interesting inverse problems in scientific computing

Algorithm 4.1 Posterior sampling procedure for the Darcy flow PDE inverse problem

-
- 1: **Input:**
 - 2: Data y , noise variance σ , MNIST generator \widehat{T} with reference measure $\eta = \mathcal{N}(0, I)$, and discrete parameter to observation map F , and pCN step size $\beta \in (0, 1)$.
 - 3: **Initialize MCMC:**
 - 4: Draw $z^{(0)} \sim \eta$, evaluate the generator $u^{(0)} = \widehat{T}(z^{(0)})$, and compute $\Phi(u^{(0)}; y)$
 - 5: **for** $i = 1$ to $N_{\text{sample size}}$ **do**
 - 6: Propose: $z' = \beta z^{(i-1)} + \sqrt{1 - \beta^2} \xi$ where $\xi \sim \eta$
 - 7: Evaluate the generator: $u' = \widehat{T}(z')$
 - 8: Compute the likelihood $\Phi(u'; y)$ by evaluating discrete PDE solver
 - 9: Compute acceptance probability: $\alpha = \min(1, \exp(\Phi(u^{(i-1)}; y) - \Phi(u'; y)))$
 - 10: With probability α accept z' and set $z^{(i)} = z'$ and collect $u^{(i)} = u'$
 - 11: Otherwise reject and set $z^{(i)} = z^{(i-1)}$ and collect $u^{(i)} = u^{(i-1)}$
 - 12: **end for**
-

concern infinite-dimensional parameters and many of our results, most notably the empirical convergence rates for Wasserstein distance do not readily extend to this setting; (ii) most of the constants in our bounds are dependent on the data y and they will deteriorate for low-likelihood data, it would be interesting to extend these to high probability bounds or bounds in expectation with respect to the data; (iii) the minimum Wasserstein analysis is removed from implementation of many generative models since the resulting optimization problem requires differentiation through an OT solver. It is interesting to extend our analysis to metrics and divergences beyond the Wasserstein distance that are more closely related to implementable generative models.

Acknowledgments. This work was supported by the National Science Foundation grants NSF-DMS-2208535 (Machine Learning for Bayesian Inverse Problems) and NSF-DMS-2337678 (CAREER: Gaussian Processes for Scientific Machine Learning: Theoretical Analysis and Computational Algorithms).

REFERENCES

- [1] B. ADCOCK AND N. HUANG, *How many measurements are enough? bayesian recovery in inverse problems with general distributions*, arXiv preprint arXiv:2505.10630, (2025).
- [2] M. AL-JARRAH, B. HOSSEINI, N. JIN, M. MARTINO, AND A. TAGHVAEI, *Error analysis of triangular optimal transport maps for filtering*, arXiv preprint arXiv:2510.19283, (2025).
- [3] M. ALBERGO, N. M. BOFFI, AND E. VANDEN-ELJNDEN, *Stochastic interpolants: A unifying framework for flows and diffusions*, Journal of Machine Learning Research, 26 (2025), pp. 1–80.
- [4] J. ALFONSO, R. BAPTISTA, A. BHAKTA, N. GAL, A. HOU, I. LYUBIMOVA, D. POCKLINGTON, J. SAJONZ, G. TRIGILA, AND R. TSAI, *A generative flow for conditional sampling via optimal transport*, arXiv preprint arXiv:2307.04102, (2023).
- [5] S. ARRIDGE, P. MAASS, O. ÖKTEM, AND C.-B. SCHÖNLIEB, *Solving inverse problems using data-driven models*, Acta Numerica, 28 (2019), pp. 1–174.
- [6] R. BAPTISTA, B. HOSSEINI, N. KOVACHKI, Y. MARZOUK, AND A. SAGIV, *An approximation theory framework for measure-transport sampling algorithms*, Mathematics of Computation, 94 (2025), pp. 1863–1909.

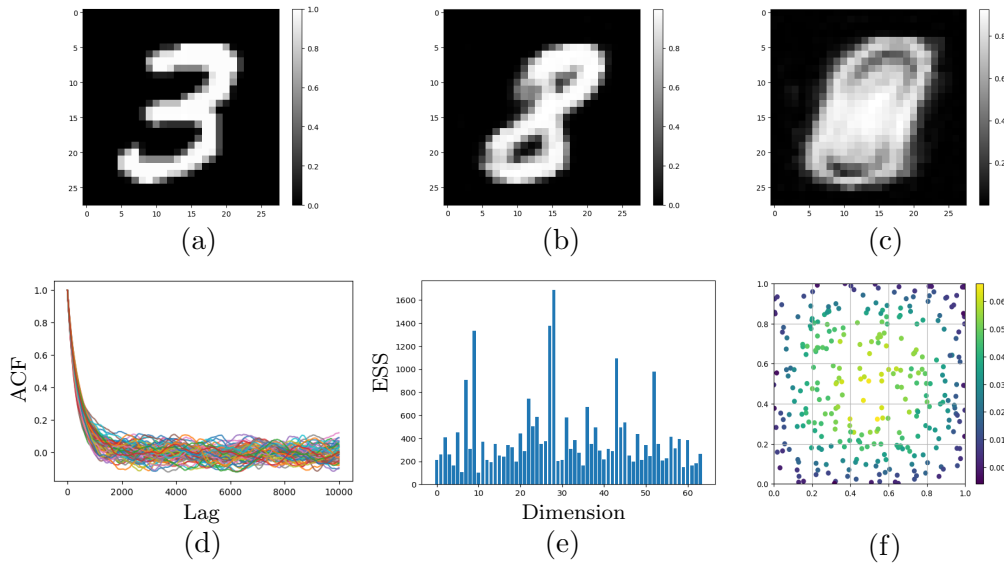


Figure 4.5: Results of the Darcy flow experiments with 20% noise-to-signal ratio: (a) the ground truth parameter; (b) posterior mean in the image space; (c) pointwise posterior standard deviation in the image space; (d) coordinate-wise autocorrelation functions (ACF) of the MCMC chain in the latent space; (e) coordinate-wise effective sample size (ESS) of the MCMC chain in the latent space; (f) the data y plotted as the noisy pointwise observations of the pressure field p arising from the true field in panel (a).



Figure 4.6: Ten independent posterior samples taken from the MCMC chain (every 10^5 steps) for our experiments with 20% noise-to-signal ratio. The samples show multiple digits, indicating the multi-modality of the posterior in the image space.

- [7] R. BAPTISTA, B. HOSSEINI, N. B. KOVACHKI, AND Y. M. MARZOUK, *Conditional sampling with monotone gans: From generative models to likelihood-free inference*, SIAM/ASA Journal on Uncertainty Quantification, 12 (2024), pp. 868–900.
- [8] J. BENTON, G. DELIGIANNIDIS, AND A. DOUCET, *Error bounds for flow matching methods*, Transactions on Machine Learning Research, (2024).
- [9] P. BOHRA, T.-A. PHAM, J. DONG, AND M. UNSER, *Bayesian inversion for nonlinear imaging models using deep generative priors*, IEEE Transactions on Computational Imaging, 8 (2023), pp. 1237–1249.
- [10] A. BORA, A. JALAL, E. PRICE, AND A. G. DIMAKIS, *Compressed sensing using generative models*, in International conference on machine learning, PMLR, 2017, pp. 537–546.
- [11] L. BUNGERT, R. RAAB, T. ROITH, L. SCHWINN, AND D. TENBRINCK, *Clip: Cheap lipschitz training of neural networks*, in International Conference on Scale Space and Variational Methods in Computer

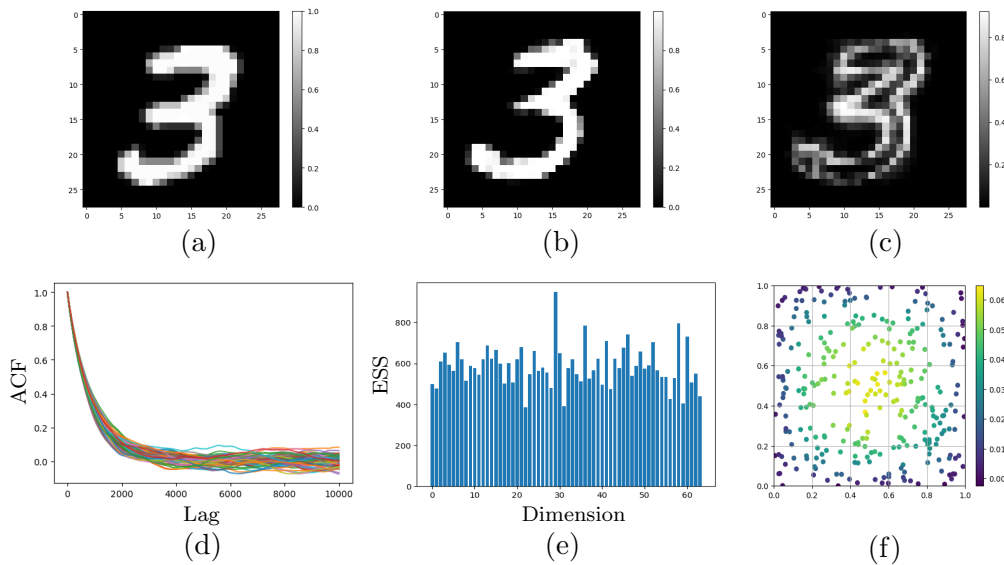


Figure 4.7: Results of the Darcy flow experiments with 10% noise-to-signal ratio: (a) the ground truth parameter; (b) posterior mean in the image space; (c) pointwise posterior standard deviation in the image space; (d) coordinate-wise autocorrelation functions (ACF) of the MCMC chain in the latent space; (e) coordinate-wise effective sample size (ESS) of the MCMC chain in the latent space; (f) the data y plotted as the noisy pointwise observations of the pressure field p arising from the true field in panel (a).



Figure 4.8: Ten independent posterior samples taken from the MCMC chain (every 10^5 steps) for our experiments with 10% noise-to-signal ratio. The samples show small variations of the digit "3", indicating the multi-modality of the posterior in the image space.

Vision, Springer, 2021, pp. 307–319.

- [12] S. CHEWI, J. NILES-WEED, AND P. RIGOLLET, *Statistical optimal transport*, Springer, 2024.
- [13] S. L. COTTER, G. O. ROBERTS, A. M. STUART, AND D. WHITE, *Mcmc methods for functions: modifying old algorithms to make them faster*, *Statistical Science*, (2013), pp. 424–446.
- [14] T. CUI, Y. M. MARZOUK, AND K. E. WILLCOX, *Data-driven model reduction for the bayesian solution of inverse problems*, *International Journal for Numerical Methods in Engineering*, 102 (2015), pp. 966–990.
- [15] M. DASHTI AND A. M. STUART, *The bayesian approach to inverse problems*, in *Handbook of uncertainty quantification*, Springer, 2015, pp. 1–118.
- [16] A. G. DIMAKIS, A. BORA, D. VAN VEEN, A. JALAL, S. VISHWANATH, AND E. PRICE, *Deep generative models and inverse problems*, *Mathematical Aspects of Deep Learning*, 400 (2022).

- [17] V. DIVOL, J. NILES-WEED, AND A.-A. POOLADIAN, *Optimal transport map estimation in general function spaces*, The Annals of Statistics, 53 (2025), pp. 963–988.
- [18] M. DUFF, N. D. CAMPBELL, AND M. J. EHRHARDT, *Regularising inverse problems with generative machine learning models*, Journal of Mathematical Imaging and Vision, 66 (2024), pp. 37–56.
- [19] N. FOURNIER AND A. GUILLIN, *On the rate of convergence in wasserstein distance of the empirical measure*, Probability theory and related fields, 162 (2015), pp. 707–738.
- [20] A. GARBUNO-INIGO, T. HELIN, F. HOFFMANN, AND B. HOSSEINI, *Bayesian posterior perturbation analysis with integral probability metrics*, arXiv preprint arXiv:2303.01512, (2023).
- [21] A. GELMAN, J. B. CARLIN, H. S. STERN, D. B. DUNSON, A. VEHTARI, AND D. B. RUBIN, *Bayesian Data Analysis*, CRC Press, 2013.
- [22] I. GOODFELLOW, J. POUGET-ABADIE, M. MIRZA, B. XU, D. WARDE-FARLEY, S. OZAIR, A. COURVILLE, AND Y. BENGIO, *Generative adversarial networks*, Communications of the ACM, 63 (2020), pp. 139–144.
- [23] I. GULRAJANI, F. AHMED, M. ARJOVSKY, V. DUMOULIN, AND A. C. COURVILLE, *Improved training of wasserstein gans*, Advances in neural information processing systems, 30 (2017).
- [24] A. HABRING AND M. HOLLER, *A generative variational model for inverse problems in imaging*, SIAM Journal on Mathematics of Data Science, 4 (2022), pp. 306–335.
- [25] B. HOSSEINI, *Well-posed bayesian inverse problems with infinitely divisible and heavy-tailed prior measures*, SIAM/ASA Journal on Uncertainty Quantification, 5 (2017), pp. 1024–1060.
- [26] B. HOSSEINI, A. W. HSU, AND A. TAGHVAEI, *Conditional optimal transport on function spaces*, SIAM/ASA Journal on Uncertainty Quantification, 13 (2025), pp. 304–338.
- [27] B. HOSSEINI AND N. NIGAM, *Well-posed bayesian inverse problems: Priors with exponential tails*, SIAM/ASA Journal on Uncertainty Quantification, 5 (2017), pp. 436–465.
- [28] D. Z. HUANG, J. HUANG, AND Z. LIN, *Convergence analysis of probability flow ode for score-based generative models*, IEEE Transactions on Information Theory, (2025).
- [29] J. HUANG, Y. JIAO, Z. LI, S. LIU, Y. WANG, AND Y. YANG, *An error analysis of generative adversarial networks for learning distributions*, Journal of machine learning research, 23 (2022), pp. 1–43.
- [30] J.-C. HÜTTER AND P. RIGOLLET, *Minimax estimation of smooth optimal transport maps*, The Annals of Statistics, 49 (2021).
- [31] N. J. IRONS, M. SCETBON, S. PAL, AND Z. HARCHAOU, *Triangular flows for generative modeling: Statistical consistency, smoothness classes, and fast rates*, in International Conference on Artificial Intelligence and Statistics, PMLR, 2022, pp. 10161–10195.
- [32] A. JALAL, M. ARVINTE, G. DARAS, E. PRICE, A. G. DIMAKIS, AND J. TAMIR, *Robust compressed sensing mri with deep generative priors*, Advances in neural information processing systems, 34 (2021), pp. 14938–14954.
- [33] J. P. KAIPIO AND E. SOMERSALO, *Statistical and computational inverse problems*, Springer, 2005.
- [34] M. C. KENNEDY, A. O’HAGAN, AND N. HIGGINS, *Bayesian analysis of computer code outputs*, Quantitative methods for current environmental issues, (2002), pp. 227–243.
- [35] D. P. KINGMA AND P. DHARIWAL, *Glow: Generative flow with invertible 1×1 convolutions*, Advances in neural information processing systems, 31 (2018).
- [36] I. KOBYZEV, S. PRINCE, AND M. BRUBAKER, *Normalizing flows: An introduction and review of current methods.*, IEEE Transactions on Pattern Analysis and Machine Intelligence, 43 (2021), pp. 3964–3979.
- [37] J. LATZ, *On the well-posedness of bayesian inverse problems*, SIAM/ASA Journal on Uncertainty Quantification, 8 (2020), pp. 451–482.
- [38] R. LAUMONT, V. D. BORTOLI, A. ALMANSA, J. DELON, A. DURMUS, AND M. PEREYRA, *Bayesian imaging using plug & play priors: when langevin meets tweedie*, SIAM Journal on Imaging Sciences, 15 (2022), pp. 701–737.
- [39] T. LIANG, *How well generative adversarial networks learn distributions*, Journal of Machine Learning Research, 22 (2021), pp. 1–41.
- [40] Y. LIPMAN, R. T. CHEN, H. BEN-HAMU, M. NICKEL, AND M. LE, *Flow matching for generative modeling*, in 11th International Conference on Learning Representations (ICLR), 2023.
- [41] J.-M. LUECKMANN, J. BOELTS, D. GREENBERG, P. GONCALVES, AND J. MACKE, *Benchmarking simulation-based inference*, in International conference on artificial intelligence and statistics, PMLR, 2021, pp. 343–351.

- [42] S. LUNZ, O. ÖKTEM, AND C.-B. SCHÖNLIEB, *Adversarial regularizers in inverse problems*, Advances in neural information processing systems, 31 (2018).
- [43] Y. MARZOUK, Z. R. REN, S. WANG, AND J. ZECH, *Distribution learning via neural differential equations: a nonparametric statistical perspective*, Journal of Machine Learning Research, 25 (2024), pp. 1–61.
- [44] S. MUKHERJEE, S. DITTMER, Z. SHUMAYLOV, S. LUNZ, O. ÖKTEM, AND C.-B. SCHÖNLIEB, *Data-driven convex regularizers for inverse problems*, in ICASSP 2024-2024 IEEE International Conference on Acoustics, Speech and Signal Processing (ICASSP), IEEE, 2024, pp. 13386–13390.
- [45] S. MUKHERJEE, A. HAUPTMANN, O. ÖKTEM, M. PEREYRA, AND C.-B. SCHÖNLIEB, *Learned reconstruction methods with convergence guarantees: A survey of concepts and applications*, IEEE Signal Processing Magazine, 40 (2023), pp. 164–182.
- [46] A. MÜLLER, *Integral probability metrics and their generating classes of functions*, Advances in applied probability, 29 (1997), pp. 429–443.
- [47] G. ONGIE, A. JALAL, C. A. METZLER, R. G. BARANIUK, A. G. DIMAKIS, AND R. WILLET, *Deep learning techniques for inverse problems in imaging*, IEEE Journal on Selected Areas in Information Theory, 1 (2020), pp. 39–56.
- [48] R. OROZCO, A. SIAHKOOHI, M. LOUBOUTIN, AND F. J. HERRMANN, *Aspire: iterative amortized posterior inference for bayesian inverse problems*, Inverse Problems, 41 (2025), p. 045001.
- [49] H. OWHADI, C. SCOVEL, AND T. SULLIVAN, *On the brittleness of bayesian inference*, siam REVIEW, 57 (2015), pp. 566–582.
- [50] B. PANDEY, B. HOSSEINI, P. BATLLE, AND H. OWHADI, *Diffeomorphic measure matching with kernels for generative modeling*, SIAM Journal on Mathematics of Data Science, 7 (2025), pp. 937–964.
- [51] D. V. PATEL, D. RAY, AND A. A. OBERAI, *Solution of physics-based bayesian inverse problems with deep generative priors*, Computer Methods in Applied Mechanics and Engineering, 400 (2022), p. 115428.
- [52] S. RIEDMAIER, B. DANQUAH, B. SCHICK, AND F. DIERMEYER, *Unified framework and survey for model verification, validation and uncertainty quantification*, Archives of Computational Methods in Engineering, 28 (2021), pp. 2655–2688.
- [53] V. SHAH AND C. HEGDE, *Solving linear inverse problems using gan priors: An algorithm with provable guarantees*, in 2018 IEEE international conference on acoustics, speech and signal processing (ICASSP), IEEE, 2018, pp. 4609–4613.
- [54] S. SINGH, A. UPPAL, B. LI, C.-L. LI, M. ZAHEER, AND B. PÓCZOS, *Nonparametric density estimation under adversarial losses*, Advances in Neural Information Processing Systems, 31 (2018).
- [55] Y. SONG, L. SHEN, L. XING, AND S. ERMON, *Solving inverse problems in medical imaging with score-based generative models*, in NeurIPS 2021 Workshop on Deep Learning and Inverse Problems.
- [56] B. SPRUNGK, *On the local lipschitz stability of bayesian inverse problems*, Inverse Problems, 36 (2020), p. 055015.
- [57] A. M. STUART, *Inverse problems: a bayesian perspective*, Acta numerica, 19 (2010), pp. 451–559.
- [58] T. SULLIVAN, *Well-posed bayesian inverse problems and heavy-tailed stable quasi-banach space priors*, Inverse Problems and Imaging, 11 (2017), pp. 857–874.
- [59] T. J. SULLIVAN, *Introduction to uncertainty quantification*, vol. 63, Springer, 2015.
- [60] B. TAHMASEBI AND S. JEGELKA, *Sample complexity bounds for estimating probability divergences under invariances*, in Proceedings of the 41st International Conference on Machine Learning, 2024, pp. 47396–47417.
- [61] R. TANG AND Y. YANG, *Minimax rate of distribution estimation on unknown submanifolds under adversarial losses*, The Annals of Statistics, 51 (2023), pp. 1282–1308.
- [62] S. V. VENKATAKRISHNAN, C. A. BOUMAN, AND B. WOHLBERG, *Plug-and-play priors for model based reconstruction*, in 2013 IEEE global conference on signal and information processing, IEEE, 2013, pp. 945–948.
- [63] C. VILLANI ET AL., *Optimal transport: old and new*, vol. 338, Springer, 2009.
- [64] A. VIRMAUX AND K. SCAMAN, *Lipschitz regularity of deep neural networks: analysis and efficient estimation*, Advances in neural information processing systems, 31 (2018).
- [65] C. R. VOGEL, *Computational methods for inverse problems*, SIAM, 2002.
- [66] S. WANG AND Y. MARZOUK, *On minimax density estimation via measure transport*, arXiv preprint arXiv:2207.10231, (2022).
- [67] A. ZAMMIT-MANGION, M. SAINSBURY-DALE, AND R. HUSER, *Neural methods for amortized inference*,

- Annual Review of Statistics and Its Application, 12 (2025), pp. 311–335.
- [68] J. ZECH AND Y. MARZOUK, *Sparse approximation of triangular transports, part i: The finite-dimensional case*, Constructive Approximation, 55 (2022), pp. 919–986.
- [69] J. ZECH AND Y. MARZOUK, *Sparse approximation of triangular transports, part ii: The infinite-dimensional case*, Constructive Approximation, 55 (2022), pp. 987–1036.
- [70] J. ZHANG, J. YIN, AND R. WANG, *Basic framework and main methods of uncertainty quantification*, Mathematical Problems in Engineering, 2020 (2020), p. 6068203.
- [71] K. ZHANG, Y. LI, W. ZUO, L. ZHANG, L. VAN GOOL, AND R. TIMOFTE, *Plug-and-play image restoration with deep denoiser prior*, IEEE Transactions on Pattern Analysis and Machine Intelligence, 44 (2022), pp. 6360–6376.
- [72] K. ZHANG, W. ZUO, S. GU, AND L. ZHANG, *Learning deep cnn denoiser prior for image restoration*, in Proceedings of the IEEE conference on computer vision and pattern recognition, 2017, pp. 3929–3938.

Appendix A. Sequential training of WGANs. In the 2D benchmark experiment, we trained a WGAN-gp to generate the priors. In order to increase the accuracy of training result and illustrate the effect of sample size, network width, and training epochs, we applied a sequential training method to our WGAN-gp.

A.1. Default Setting for Sequential Training of WGAN-gp. Our default WGAN-gp which produced [Figure 4.1](#) was set up with following details:

- *Basic structure of a single model:* Our generator and discriminator in a single model were set to be 3 layers and each layer has width of 128. The input and output dimension of our generator were set to be 2D. After testing our training model, we noticed the discriminator training loss would be unstable with 2D input. To make the training process stable, we add a zero vectors in the input of discriminator so that the input of discriminator is 3D with output dimension to be 1D.
- *Hyper-parameters for training:* In the training process, our default setting is 10000 data points with batch size of 512, the number of total epochs is 10000. During the training, we update our generator every 20 epochs to make sure the discriminator is fully trained. Lastly, our gradient penalty weight was set to be 5 and the learning rate was 0.01. The optimizer we used was SGD.
- *Setting up for sequential training:* After setting up the single WGAN-gp, we use a loop to sequentially train 5 models G_1, \dots, G_5 . In the first step, the input data is $x_1 \sim N(0, I)$. To keep updates small and smooth, we set the output to be residual such that $y_1 = x_1 + G(x_1)$. Then, starts from G_2 , we choose the input $x_i = y_i = x_{i-1} + G(x_{i-1})$ to sequentially train G_2, \dots, G_5 . With these sequential models, our generative priors were accurate enough to illustrate the effect of sample size, network width, and training epochs.

A.2. Hyper-parameter Tuning for analyzing of effect of sample size, model width and training epochs.

- *Tuning for analyzing effect of training sample:* In the experiment of analyzing effect of training sample, we keep our WGAN-gp’s architecture with 3 layers and with width of 128. The sequential training models were kept as 5 as well. The training epochs were set to be 10000 and all other hyper-parameters were set as in [Subsection A.1](#). With those hyperparameters to be fixed, we change the number of training samples from 2^9 to 2^{13} for the distribution of swissroll and pinwheel, and from 2^{10} to 2^{14} for

the distribution of checkerboard to obtain [Figure 4.2](#).

- *Tuning for analyzing effect of network width:* In the experiment of analyzing effect of width for our WGAN-gp, we keep the training epochs to be 10000 and the number of training samples to be 10000. We also kept the number of layers for each neural network as 3 and the sequential models to be 5. With all other hyper-parameters fixed as in [Subsection A.1](#), we modified the width of the neural network from 2^4 to 2^8 to obtain [Figure 4.3](#).
- *Tuning for analyzing effect of training epochs:* In the experiment of analyzing effect of training epochs, we keep the architecture of our networks as 3 layers with width of 128 and 5 steps for sequential training models. The training samples were set to be 10000 and all other hyperparameters were set as in [Subsection A.1](#). Then, we changed our training epochs from 2^8 to 2^{12} to get [Figure 4.4](#).

Appendix B. WGANgp Training for High Dimension Experiments. In the High Dimension Experiments, we trained a WGAN-gp to generate MNIST images. Here is the detail:

- *Architecture of the network:* The generator of our WGAN-gp for high-dimensional problem has the input of dimension 64. It then has three internal layers of dimension 256, 512, and 1024. The output dimension needs to be agree with the size of MNIST image, which was 784 (28 by 28). The discriminator has the input dimension of 784 as it needs to be agree with the MNIST image dimension. It has two layers of 512 and 256, with the output dimension as 1. For both the generator and discriminator, inbetween each layers, we set the LeakyReLU activation function with the parameter to be 0.2.
- *Hyperparameters:* To train the WGAN-gp for generating MNIST image, we used the whole MNIST dataset and the batch size was 64. Our total number of epochs was 600 and we update the parameters of generator every 5 epochs. Our learning rate was 10^{-4} and the gradient penalty weight was set to be 5. Lastly, we choose Adam as our optimizer for this training task.

Appendix C. Finite Element method for Darcyflow PDE solver. To solve the Darcyflow PDE numerically, our Finite Element method was defined as follows: Since we were given the generated MNIST image as input in the size of 28 by 28, we stick with the same size for our preliminary fields in the domain $(0, 1)^2$. We applied the Dirichlet Boundary conditions in the domain and the output numerical results were still in the size of 28 by 28.

Appendix D. MCMC for sampling Darcyflow PDE solution. The MCMC algorithm for sampling the posterior were defined in [Algorithm 4.1](#). For each sampling task, we set the first 20% steps to be the burning up process in order to tuning the step size parameter β . During the burning up process, for every 100 steps, if the average acceptance rate $\alpha_{avg} > 0.4$, we set $\beta_{new} = \beta/2$; if the average acceptance rate $\alpha_{avg} < 0.2$, we set $\beta_{new} = ((1 - \beta)/2)$. Therefore, with enough burning up steps, we could control the acceptance rate after burning up to be around 0.3, which was usually a proper acceptance rate for the effectiveness of MCMC algorithm.